minerals

MDPI

Article

Provenance of the Upper Carboniferous Yanghugou Formation in the Western Margin of the Ordos Basin, China: Constraints on Paleogeography and Basin Development

Tao Zhang [1,2], Rong Chen [1,3,*], Feng Wang [1], Jianling Hu [4], Min Zhang [1], Qian Li [1], Jingyi Wu [1] and Lei Liu [1]

1 Institute of Sedimentary Geology, Chengdu University of Technology, Chengdu 610059, China; zhangtao_cq@petrochina.com.cn (T.Z.); wangfeng07@cdut.cn (F.W.); 18380364387@163.com (M.Z.); liqian6@stu.cdut.edu.cn (Q.L.); 18702822398@163.com (J.W.); liulei10owen@163.com (L.L.)
2 Exploration Department, PetroChina Changqing Oilfield Company, Xi'an 710018, China
3 Museum of Chengdu University of Technology, Chengdu 610059, China
4 Research Institute of Exploration and Development, PetroChina Changqing Oilfield Company, Xi'an 710000, China; pyxh0112_cq@petrochina.com.cn
* Correspondence: chenrong07@cdut.cn

Abstract: The Carboniferous Yanghugou Formation in the western margin of the Ordos Basin exhibits significant potential for oil and gas exploration. However, due to the influence of complex tectonic activities, there are substantial variations in stratigraphic thickness and depositional environments across the formation. The lack of a systematic source–sink comparative study has resulted in an unclear understanding of sediment sources and paleogeographic patterns, impacting the exploration for hydrocarbon accumulations. We conducted a comprehensive study of the source–sink system characteristics and paleogeography in the research area through field outcrop observations and drilling core sampling. By utilizing detrital zircon U–Pb geochronology and geochemistry, paleocurrent directions, lithofacies types, and sedimentary features, we delve into the understanding of the source–sink systems. Four major source–sink regions in the research area were identified: the Alxa, Yinshan, Alxa–Yinshan mixed and Qilian source–sink regions. The Alxa source–sink region formed a transitional delta-barrier-island sedimentary system. The northern part of the Yinshan source–sink region developed a transitional tidal-controlled delta-tidal-flat sedimentary system, while the southern deep-water area developed a shallow marine to semi-deep marine shelf sedimentary systems. The sediments of Alxa–Yinshan mixed source–sink region were deposited in a transitional tidal-controlled delta-tidal-flat barrier-island system. The Qilian source–sink region is characterized by small tidal-controlled delta-barrier-island system. From the analysis of the source–sink systems, it is inferred that the Alxa Block and the North China Craton had already merged before deposition of the late Carboniferous Yanghugou Formation. The delta sand bodies in the Alxa–Yinshan mixed source–sink region have the highest compositional and structural maturity, the best reservoir performance, and the great exploration potential.

Keywords: detrital zircon geochronology; paleogeography; source–sink system; Yanghugou Formation; North China Craton

check for updates

Citation: Zhang, T.; Chen, R.; Wang, F.; Hu, J.; Zhang, M.; Li, Q.; Wu, J.; Liu, L. Provenance of the Upper Carboniferous Yanghugou Formation in the Western Margin of the Ordos Basin, China: Constraints on Paleogeography and Basin Development. *Minerals* **2024**, *14*, 78. https://doi.org/10.3390/min14010078

Academic Editors: Hermann Kudrass and Manuel Francisco Pereira

Received: 17 November 2023
Revised: 31 December 2023
Accepted: 5 January 2024
Published: 10 January 2024

1. Introduction

The Ordos Basin is one of the most prolific hydrocarbon-generating basins in China, containing abundant hydrocarbon resources [1,2]. In recent years, a series of important upper Palaeozoic oil and gas fields, such as Shenglijing, Liujiazhuang, Majiatan, Dashuikeng, and Baiyanjing, have been discovered in the western margin of the basin, showing good prospects for oil and gas exploration. The reservoir of the Upper Carboniferous Yanghugou Formation in the western Ordos Basin has particularly large deposit thickness and good exploration potential [3–5].

The distribution of hydrocarbon is closely related to several factors, including organic matter availability and related factors of paleobioproductivity, sea-level change, provenance area, paleogeography and circulation patterns, rate of sedimentation, and paleoclimatic variability [6–8]. The structural background of the Yanghugou Formation on the western margin of the Ordos Basin is complex, and the sedimentary environments underwent frequent changes. However, there is a relative scarcity of drilling and seismic data, leading to conflicting interpretations of provenance supply and sedimentary characteristics in this region. Previous studies indicated that the Yanghugou Formation primarily represents tide-dominated-delta and barrier-coast depositional systems [9–11], while others argued for the development of shallow marine shelves and fan-delta depositional systems [12]. Previous investigations of the sedimentary environments and facies of the Yanghugou Formation were largely confined to field geological outcrops [13,14], lacking data from drilled cores. Additionally, the sedimentary facies thickness and types vary significantly across the western margin of the basin. Different periods exhibit distinct sedimentary environments, and a sole sedimentary system or model cannot adequately illustrate the depositional characteristics and evolutionary processes of sedimentary facies in the Yanghugou Formation [15]. Previous studies indicated that the northern provenance of the Upper Paleozoic in the western margin of the Ordos Basin is Alxa Block and Yinshan Ancient Land, and the southern provenance is the North Qilian and North Qinling Orogenic Belts [16,17]. However, the contribution of these potential sources is not distinguished in detail, and there are many disputes about the sedimentary pattern under different provenances [9,12,18].

In order to clarify the provenance, source–sink relationships, and paleogeographic distribution of the Yanghugou Formation on the western margin of the Ordos Basin, this study systematically analyzed a set of samples from drill cores and outcrops from the western margin of the Ordos Basin. The specific objectives of the study are as follows: (1) to elucidate the source–sink relationships related to the deposition of the Carboniferous Yanghugou Formation on the western margin of the Ordos Basin; (2) to reconstruct the distribution and evolution of paleogeography; and (3) to provide a geologic basis for oil and gas exploration.

2. Geological Setting

The western margin of the Ordos Basin is located at the junction of the Ordos Block, the Qilian Orogenic Belt, North Qinling Orogenic Belt, and the Alxa Block (Figure 1a,b) [19]. It is a hub connecting different tectonic units in the east and west of China [20]. The Ordos Block is entirely covered by Mesozoic and Cenozoic sedimentary rocks in the Ordos Basin, though available borehole and aeromagnetic data suggest the existence of a granulite facies basement of the Archean and Lower Proterozoic beneath the overlying Ordos Basin [21]. The North Qinling Belt is bounded by the Luonan–Luanchuan Fault to the north and the Shangdan Suture to the south (Figure 1a) and represents a composite orogenic belt from the Middle Neoproterozoic to the Cenozoic. The North Qilian Orogenic Belt is an elongate, NW–SE-trending belt (Figure 1a), which is a typical oceanic suture zone from Neoproterozoic to Paleozoic [22]. The Alxa Block is triangular in shape (Figure 1a) and is a composite ribbon continent from Neoarchean to Paleoproterozoic. There are multi-stage magmatism and ductile deformation in the Alxa Block from the Ordovician to the Early Permian [23]. Influenced by the joint effects of the passive continental margin of the Qilian-Qinling Orogenic Belt and the active continental margin of the ancient Alxa Block, the thrust belt on the western margin of the Ordos Basin belonged to the Qilian Sea during the Upper Carboniferous. It represents a rift basin subjected to north–south compression and western extension [24]. During the sedimentation period of the Yanghugou Formation, the Yinshan Ancient Land in the northern part of the study area is in the stage of southward subduction of the Paleo-Asian Ocean [25]; the Qinling Orogenic Belt in the southern part is in the stage of continent–continent collision [26]; and the northwestern margin is in the stage of reactivation of the Helan aulacogen [27], from which seawater enters the study area.

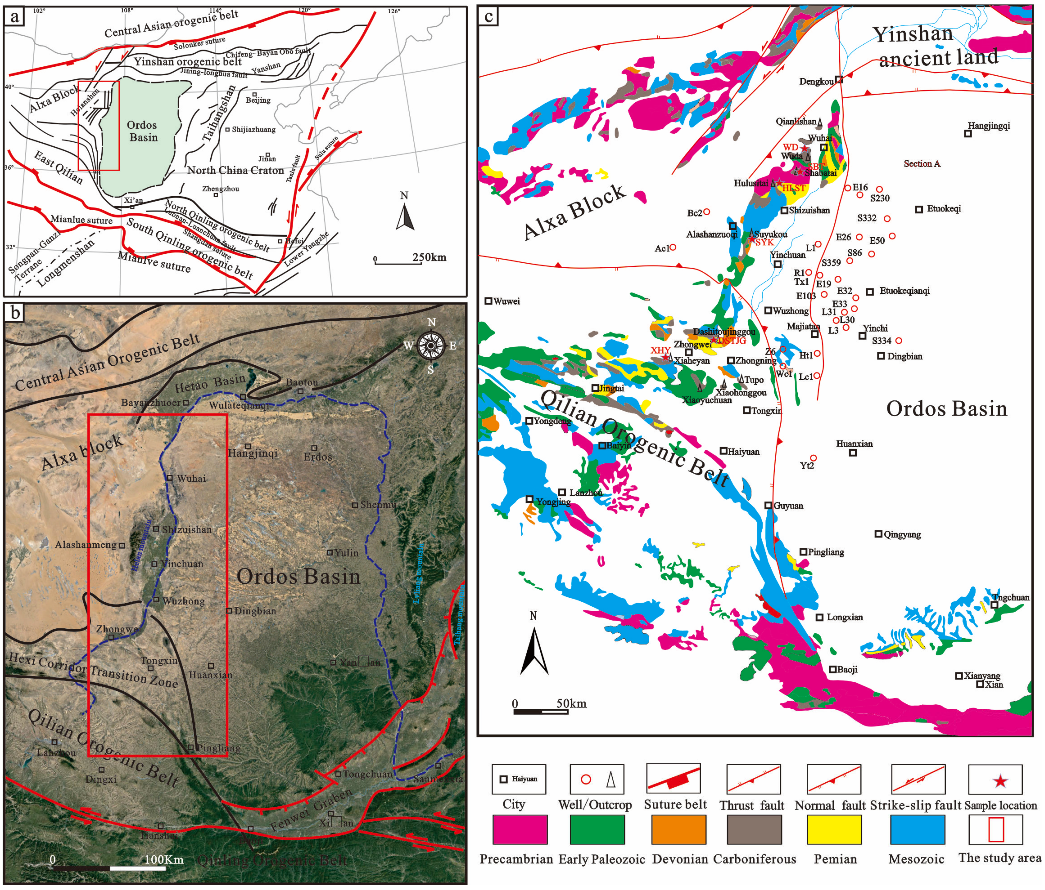

Figure 1. Study area of the western margin of the Ordos Basin. (**a**) Structural map with the location of North China Craton and Ordos Basin [19]. (**b**) Satellite image of the western margin of the Ordos Basin. (**c**) Geological map with location of the sampling sites in the Ordos Basin.

During the deposition of the Yanghugou Formation, the subsidence magnitude on the western margin of the basin exhibited extreme variability in space, evidenced by significant differences in sediment thickness [28]. The sediment thickness ranged from tens of meters to over a thousand meters, overall thickening westward. A north–south-trending central ancient uplift, extending across the western part of the basin in the vicinity of Etuokeqi, Dingbian, and Huanxian, caused a physical barrier between the Qilian Sea and the North China Sea. The western Qilian Sea acted as a rift basin, while the eastern North China Sea formed a continental shelf basin. During the Carboniferous, the extent of marine transgression gradually expanded, and seawater converged from both the east and west sides, overlaying the uplifted region in the central part of the Ordos Basin. Eventually, during the late stages of Yanghugou Formation deposition, it breached, forming a shallow sea basin along the northern edge of the North China Craton [29].

Carboniferous deposition within the Qilian Sea on the western margin of the Ordos Basin is older than that on the eastern margin of the basin [10,30]. The underlying strata of the Yanghugou Formation consist of the Carboniferous Jingyuan Formation, characterized mainly by black shale. Overlying these layers is the Permian Taiyuan Formation, composed mainly of gray-white fine-grained sandstone, gray-black mudstone, and carbonaceous mudstone. The Yanghugou Formation is roughly equivalent to the eastern Benxi Formation in the central basin (Figure 2). The Yanghugou Formation is mostly composed of rhythmic interbedding of gray-white (with gravel) quartz sandstone, gray-black fine-grained sandstone, and black shale, with few intercalations of gray limestone and thin coal seams [29].

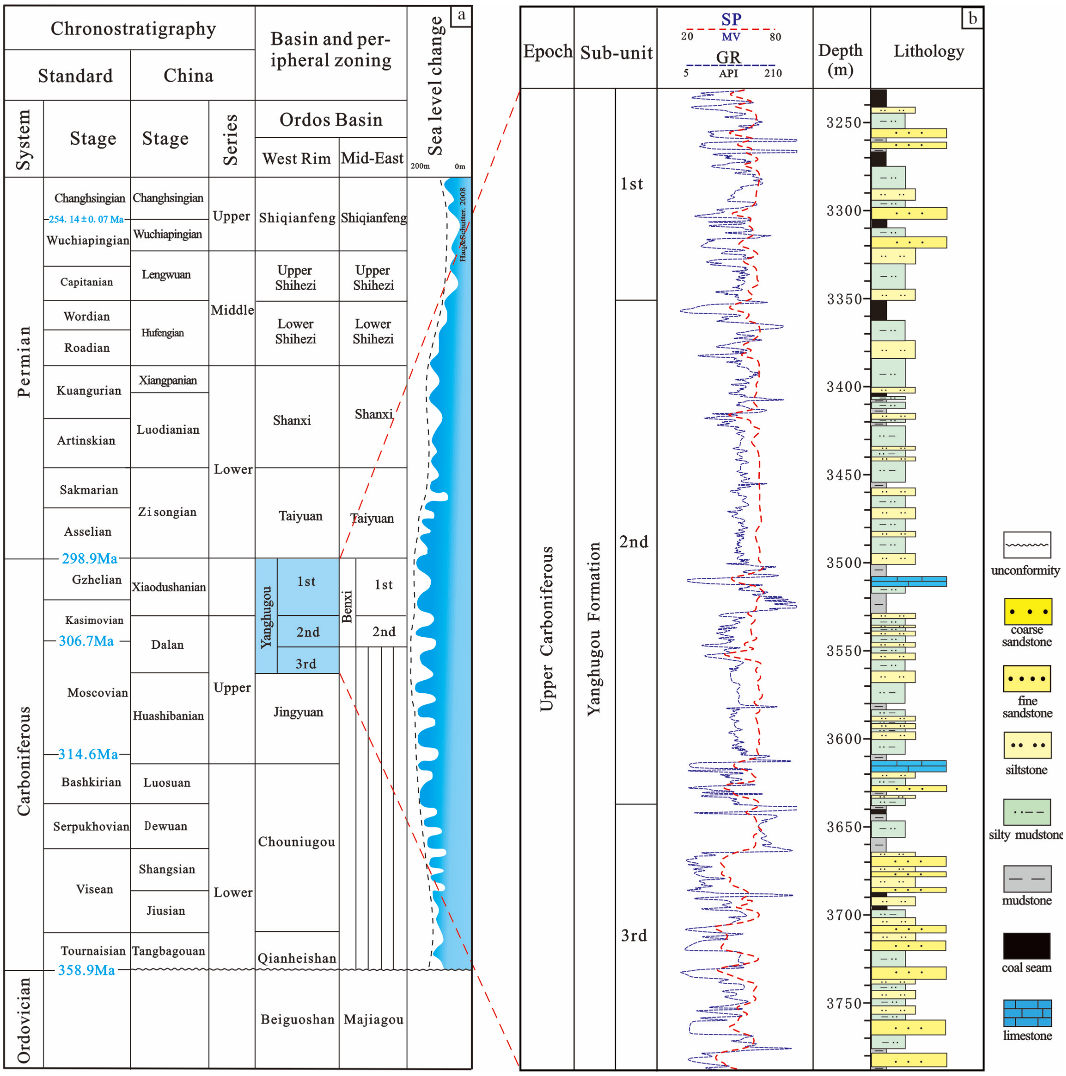

Figure 2. Stratigraphic characteristics of the Yanghugou Formation. (**a**) Distribution of Carboniferous strata in the western margin and surrounding areas of the Ordos Basin. Chronostratigraphic framework according to Shen et al. [31]; Sea-level change curve according to Haq and Schutter [32]. (**b**) Comprehensive lithological characteristics of the Yanghugou Formation in Well Z6 on the western margin of the Ordos Basin. SP—spontaneous potential logging curve; MV—millivolt; GR—natural gamma log curve; and API—American Petroleum Institute Standard.

The identification of different sections of the Yanghugou Formation is based on paleontological characteristics [15]. The lower section of the Yanghugou Formation is characterized by a notable increase in the abundance of Radiizonates and the simultaneous appearance of Apiculatisporis for the first time. The middle section of this formation exhibits a diverse range of fern spores, including Trilete spores, along with the presence of single-saccate pollen Florinites, Potonisporites, and bisaccate pollen. The upper section of the Yanghugou Formation is characterized by a significant presence of the spore–pollen assemblage Florinites junior—Laevigatosporites vulgaris (Figure 3). Additionally, there are distinct differences in Fusulina and Triticites in the middle section of the Yanghugou Formation compared to the overlying Taiyuan Formation, which is marked by the presence of Sphaeroschwagerina.

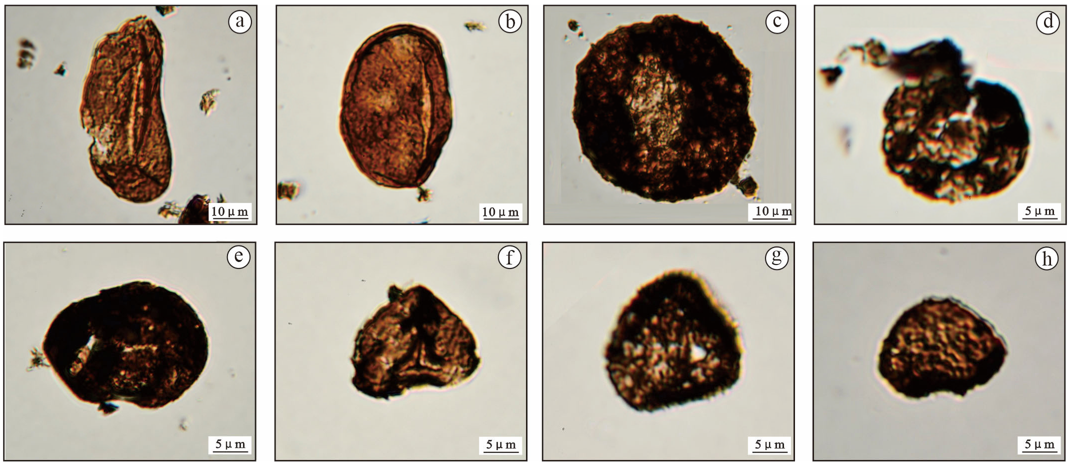

Figure 3. Fossil spores of ferns of the Yanghugou Formation from Well Z6 in the western margin of the Ordos Basin. (**a**) *Laevigatosporites* sp., 3342 m; (**b**) *Laevigatosporites robustus*, 3342 m; (**c**) *Florinites* sp., 3356 m; (**d**) *Florinites* sp., 3400 m; (**e**) *Potonieisporites elegans*, 3460 m; (**f**) *Leiotriletes levis*, 3615 m; (**g**) *Apiculatisporis* sp., 3640 m; and (**h**) *Cyclogranisporites* sp., 3700 m.

3. Materials and Methods

Sedimentological and detrital zircon geochronology methods were employed to conduct provenance and paleogeographic analyses of the Yanghugou Formation.

3.1. Sedimentology

The sedimentological analysis primarily focused on describing sedimentary facies types and their evolutionary relationships through indicators such as color, lithology, texture, sedimentary structures, and fossils from outcrops and drill cores. Thin sections for sedimentary petrography were examined using a Leica polarizing microscope and SEM by using Quanta250 FEG in the State Key Laboratory of Oil and Gas Reservoir Geology and Exploitation (Chengdu University of Technology).

Cross-bedding measurements to determine paleocurrent directions [15,33] were restored by stereographic projection and rose map.

3.2. Detrital Zircon Geochronology and Geochemistry

Zircons were separated from 3 kg hand specimens using conventional heavy-liquid and magnetic techniques at the Langfang Regional Geological Survey, Hebei Province, China. Handpicked zircon grains were mounted in epoxy resin and polished. All the zircons were photographed in transmitted and reflected light to characterize external morphology. Back-scattered electron (BSE) and cathodoluminescence (CL) images were obtained on a JEOL JXA-8100 electron microprobe. The LA-ICP-MS U–Pb isotope and trace element analyses were performed using a RESOlution 193 excimer laser ablation system coupled to an Agilent 7700 quadrupole ICP-MS in the GeoHistory Facility, JdLC, Curtin University, Western Australia. For detailed steps and handling methods, see Barham et al. [34] and Rong et al. [34]. For trace element determination, matrix-matched, well-characterised zircon GJ-1 was used as the primary reference material for correction of instrument drift and calculation of most elemental abundances. Stoichiometric values were taken from webmineral.com (accessed on) [35]. The $^{206}Pb/^{238}U$ ages for younger zircons (<1500 Ma) were calculated using 91,500 as the primary reference material, whereas OGC [36] was the primary reference for older zircons (>1500 Ma) [37]. Detrital zircon data with concordance values (($^{206}Pb/^{238}U$) age/($^{207}Pb/^{235}U$) age × 100%) of 70%–130% were used in the discussion below.

4. Sedimentary Characteristics

4.1. Lithofacies Types

The sediment transport modes, hydraulic conditions, and sedimentary process mechanisms can be judged according to lithofacies [15]. Through the observation of samples from 12 outcrops and 28 drill cores, 16 lithofacies types were identified in the Yanghugou Formation on the western edge of the Ordos Basin (Table 1).

Table 1. Summary of lithofacies types of Yanghugou Formation in western margin of the Ordos Basin.

Code	Lithofacies	Description	Depositional Process
Gm	Massive conglomerate facies	Mainly poorly sorted conglomerate containing coarse-grained sandstone.	High-energy channel lag sedimentation
Gp	Planar cross-bedding conglomerate facies	Moderate to good sorting of pebbles, with a moderate to good degree of rounding and exhibiting imbricated structures.	High-energy channel aggradation sedimentation
St	Trough cross-bedding sandstone facies	Moderate to good sorting of medium- to coarse-grained sandstone with development of trough cross-bedding	River cutting, migration, and filling sedimentation
Sp	Planar cross-bedding sandstone facies	Moderate to good sorting of medium-grained sandstone, with the development of planar cross-bedding.	Vertical and lateral aggradation of river channels
Sm	Massive sandstone facies	Poorly sorted medium- to fine-grained sandstone.	Rapid sediment accumulation
Sh	Parallel-laminated sandstone facies	Well-sorted medium- to fine-grained sandstone with well-developed parallel bedding.	Transport of bed sediment with high flow regime and flat surface
Sl	Swash cross-bedding sandstone facies	Well-sorted, well-rounded medium- to coarse-grained sandstone with development of low-angle cross-bedding.	Reciprocating scouring of bidirectional water flow
Sf	Herringbone cross-bedding sandstone facies	Moderately to well-sorted, medium- to coarse-grained sandstone with development of herringbone cross-bedding. Local presence of clay layers.	Tidal environment, formed by bidirectional water flow migration
Fr	Ripple cross-bedding siltstone facies	Well-sorted siltstone with developed ripple cross-laminated.	Formed by current traction under low hydrodynamic forces
Fcf	Flaser bedding siltstone facies	Moderately sorted fine-grained sandstone to siltstone. Sediments are mainly composed of sand, with thin mud layers distributed discontinuously.	High-energy tidal environment
Fcw	Wavy cross-bedding siltstone facies	Moderately sorted fine-grained sandstone to siltstone with thin layers of mud	Moderate energy tidal environment
Fcl	Lenticular bedding siltstone facies	Argillaceous siltstone, which consists of isolated lenses and ripples of sand set in a mud matrix	Low-energy tidal environment
Mh	Horizontal bedding mudstone facies	Dark gray, gray-black mudstone	Suspended sediments under quiet water, deep water in situ deposition
Mc	Carbonaceous mudstone facies	Gray-black to black mudstone	Swamp depositional environment
C	Coal seam and coal line	Coal seams, partially containing plant stems and fragments	Swamp depositional environment [38]
Lm	Massive marl facies	Limestone and marlstone, some of which contain bioclasts	Lagoon- or carbonate-restricted platform

4.2. Sedimentary Facies Characteristics

Based on the original sedimentological features, four sedimentary facies, namely delta, estuarine bay tidal flat, barrier coast, and shelf, have been identified within the Yanghugou Formation sedimentary system. These are further subdivided into various sub-facies types, such as delta plain distributary channels, tide-influenced delta-front subaqueous distributary channels, tidal channels, tidal sandbars, sand flats, mixed flat, barrier sandbars, lagoons, and shelves (Figures 4 and 5).

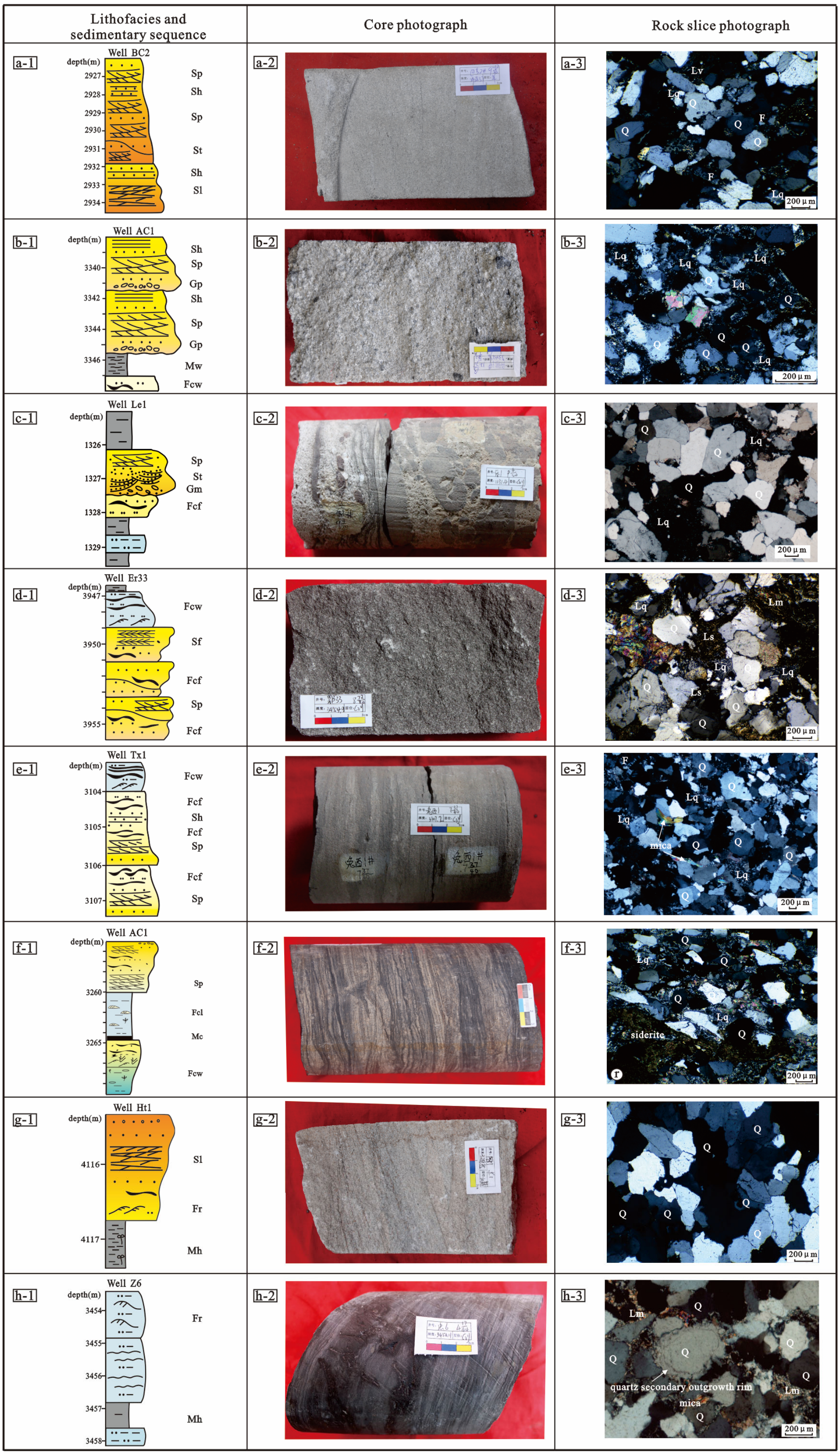

Figure 4. Sedimentary Microfacies, Depositional Sequences, Outcrops, and Core Characteristics of the Yanghugou Formation in the western margin of the Ordos Basin. (**a-1**). Delta plain distributary channel microfacies depositional sequence, BC 2 well; (**a-2**). Tabular cross-bedded sandstone, BC 2 well,

2926.32 m; (**a-3**). Feldspathic litharenite sandstone with good sorting and moderate rounding, BC 2 well, 2925.5 m, cross-polarized light. (**b-1**). Tide-influenced delta-front subaqueous distributary channel microfacies, AC 1 well; (**b-2**). Tabular cross-bedded medium to coarse sandstone, AC 1 well, 3340.92 m; (**b-3**). Lithic quartz sandstone with sub-angular to subrounded grains, AC 1 well, 3343.6 m, cross-polarized light. (**c-1**). Tidal-channel microfacies depositional sequence, L1 well; (**c-2**). Gray-white coarse-grained quartz sandstone with basal scour mud clasts, L1 well; (**c-3**). Medium-coarse lithic quartz sandstone with moderate sorting and good rounding, L1 well, 1326.9 m, cross-polarized light. (**d-1**). Tidal sandbar microfacies depositional sequence, E 33 well; (**d-2**). Gray-black medium-coarse lithic quartz sandstone; (**d-3**). Lithic quartz sandstone with good sorting and moderate rounding, E 33 well, 3954.9 m, cross-polarized light. (**e-1**). Sand flat microfacies depositional sequence, TX 1 well; (**e-2**). Ripple cross-lamination, TX 1 well; (**e-3**). Lithic quartz sandstone with moderate sorting and moderate to poor rounding, TX 1 well, 3104.2 m, cross-polarized light. (**f-1**). Mixed flat and mudflat microfacies depositional sequence, AC 1 well; (**f-2**). Sand–mud interbeds with lens-shaped bedding, AC 1 well, 3343.6 m; (**f-3**). Lithic quartz sandstone with pyrite bands, AC 1 well, 3260.1 m, cross-polarized light. (**g-1**). Barrier-island-lagoon microfacies depositional sequence, HT 1 well; (**g-2**). Low-angle cross-bedded quartz sandstone, AC 1 well, 3259.95 m; (**g-3**). Quartz sandstone with well sorting, HT 1 well, 4116.7 m, cross-polarized light. (**h-1**). Shelf microfacies depositional sequence, Z6 well; (**h-2**). Gray-black coarse-grained quartz sandstone with wavy bedding, Z6 well, 3453.8 m; (**h-3**). Lithic quartz sandstone with tight grain contacts and quartz overgrowths, Z6 well, 3455.5 m, cross-polarized light. Quartz (Q), feldspar (F), volcanic rock fragments (Lv), sedimentary rock fragments (Ls), quartzite fragments (Ls), and metamorphic rock fragments (Lm).

4.2.1. Delta

The delta plain distributary channel sediments were primarily distributed in the northern part of the study area, including the Wuda profile (Figure 5a) and the upper section of the Yanghugou Formation in the BC 2 well in the northwest (Figure 4(a-1)). The lithology is mainly composed of medium- to coarse-grained sandstone, with relatively little mud content. Vertically, it exhibits a distinct fining-upward sequence. Typically, the bottom of the stratigraphic sequence has scour surfaces, and the development of massive conglomerate facies (Gm) indicate deposition in riverbeds with backflow. Above this, trough cross-bedding sandstone facies (St), planar cross-bedding sandstone facies (Sp), and parallel-laminated sandstone facies (Sh) successively develop. This sequence reflects a unidirectional water flow, with a decrease in flow intensity from high- to low-flow conditions, indicating sedimentary processes associated with river channel incision and migration. The sandstone clastic components are primarily composed of quartz, quartz rock fragments, and feldspar, exhibiting good sorting and medium roundness, which also reflect the characteristics of strong water flow energy in deposition.

Tidal-influenced delta-front subaqueous distributary channel deposits are well developed in the northern part of the study area, including the upper part of the Hulusitai profile (Figure 5b) in the Yanghugou Formation and the middle section of the Yanghugou Formation in Well AC 1 (Figure 4(b-1)). The lithology is primarily composed of medium- to coarse-grained sandstone, fine-grained sandstone, and siltstone. Vertically, it exhibits an overall fining-upward structure. At the bottom of the stratigraphic sequence, there is a matrix-supported massive conglomerate facies (Gm) or planar cross-bedding conglomerate facies (Gp), where the gravel is sub-angular, and sorting ranges from moderate to poor. The gravel layer has strong erosional contact with the underlying mudstone. Above the gravel layer, there are successive developments of planar cross-bedding sandstone facies (Sp), parallel-laminated sandstone facies (Sh), and wavy cross-bedding siltstone facies (Fcw). At the top of the sedimentary sequence, tidal double-clay layers and tidal bundle sequences are observed, with occasional small-scale tidal-channel incisions. These features reflect that the lower section of this sedimentary sequence is primarily controlled by river processes, while the upper part is influenced by tidal effects. The clastic components are predominantly composed of quartz and siliceous rock fragments, exhibiting moderate sorting and sub-angular to sub-rounded shapes, indicating moderate to relatively strong water flow energy.

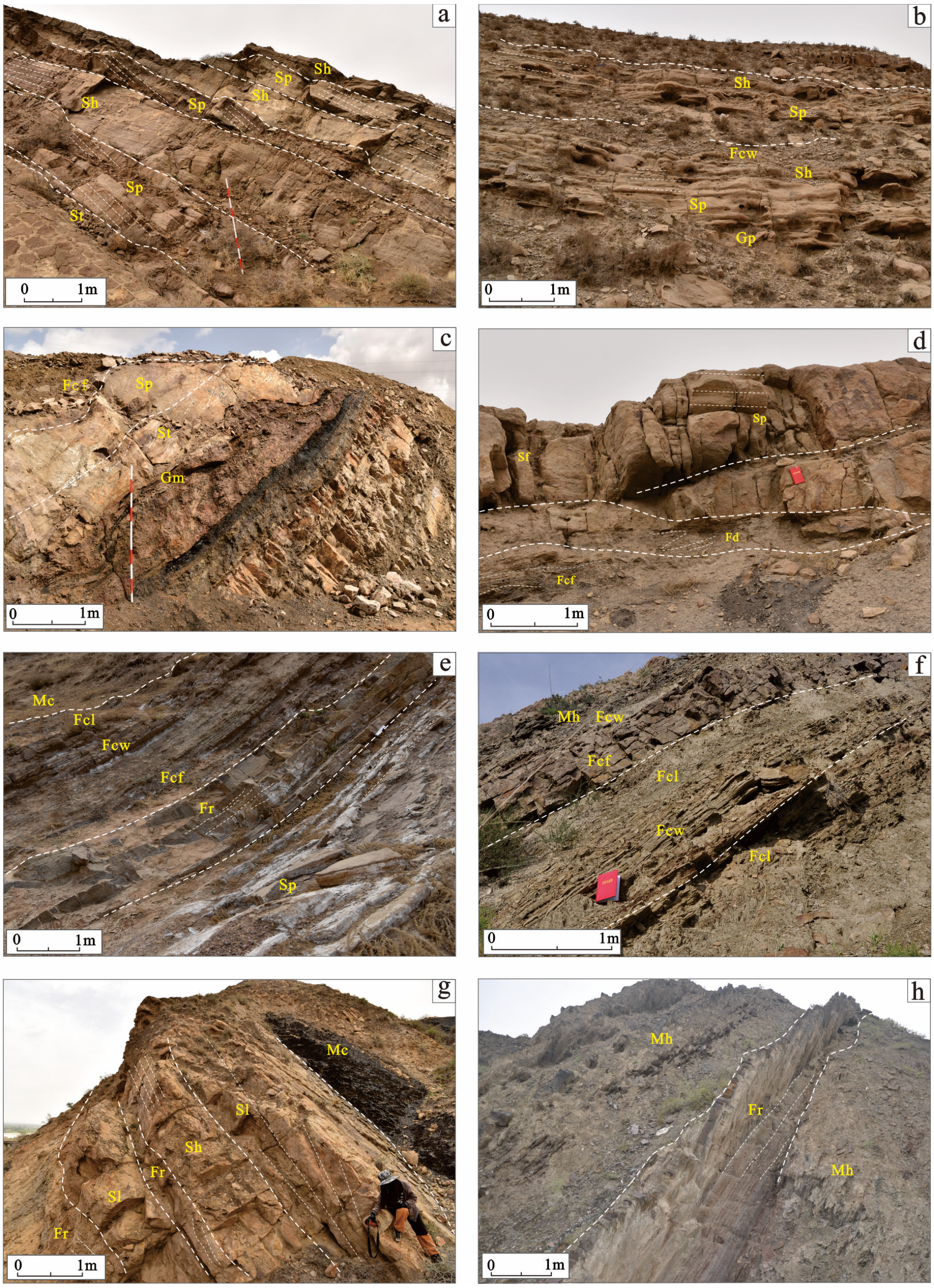

Figure 5. Outcrops of the Yanghugou Formation in the western margin of the Ordos Basin. (**a**). Delta plain distributary channel outcrop, Wuda profile; (**b**). Tide-influenced delta-front subaqueous distributary channel, Hulusitai profile; Tidal-channel microfacies depositional sequence, L1 well; (**c**). Estuarine bay tidal-channel deposition, Wuda profile; (**d**). Tidal sandbar deposition, Wuda profilI (**e**). Sand flat deposition, Tupo profile; (**f**). Mixed flat mudflat deposition, Xiaheyan profile; (**g**). Barrier-island-lagoon deposition, Xiaheyan profile; and (**h**). Shelf deposition, Dashitoujinggou profile.

4.2.2. Estuarine Bay Tidal Flat

Coastal tidal effects are mostly developed on the leeward side of barrier islands or sand dams, near the larger barrier-free walls, and the fringes of estuaries and lagoons [39]. Tidal-controlled estuaries are affected by the dual effects of rivers and tides, but tidal action plays a major control role. The Shabatai profiles in the northern part of the study area, the Xiaheyan profile in the south, and the drilling cores in the east all show important tidal deposits. According to its sedimentary characteristics, the tidal channel, tidal sand bar, sand flat and mixed flat are identified in the estuarine bay tidal flat.

Tidal-channel deposits are well developed in the northern Wuda profile (Figure 5c) and the middle section of the Yanghugou Formation in well L1 (Figure 4(c-1)). It is mainly composed of medium- to coarse-grained sandstone with minor interbedded mudstone. Vertically, the sequence exhibits an overall normal grading structure. Irregular scour surfaces are commonly found at the bottom of the stratigraphic sequence, where massive conglomerate facies (Gm) develop above the scour surfaces. In the middle section, there are trough cross-bedding sandstone facies (St), massive sandstone facies (Sm), and flaser bedding siltstone facies (Fcf) or herringbone cross-bedding sandstone facies (Sf). The lower section consists of gravelly facies, trough cross-bedded sandstone, and blocky-bedded sandstone, mainly representing fluvial deposits. The clastic components are predominantly quartz and quartzose rock fragments, showing moderate sorting and good rounding, indicating relatively strong water flow energy. In the upper section of the Yanghugou Formation, the scale of bedding decreases, the thickness of the layers becomes thinner, and tidal laminations or feathered cross-bedded sandstone develops, indicating a transition from fluvial to tidal deposits influenced by bidirectional tidal currents in a tidal environment.

Tidal sand bars develop in the offshore, subtidal high-energy zone, typically forming under conditions of extensive marine transgression and a large tidal range background [40]. They are significantly modified by tidal currents, storm surges, and other factors. In the central part of the study area, typical tidal sand bars are well developed in the Wuda profile (Figure 5d) and the upper section of the Yanghugou Formation in well E33 (Figure 4(d-1)) in the Yanghugou Formation. It is mainly composed of medium sandstone with frequent interbedded mudstone layers. In terms of grain size, there is a slight upward coarsening trend. The lower section exhibits the development of flaser bedding siltstone facies (Fcf). In the upper section, herringbone cross-bedding sandstone facies (Sf) and planar cross-bedding sandstone facies (Sp) are developed. Fluid mud layers are observed within the sandstone. The clastic components in the sandstone are predominantly quartz and quartzose rock fragments, exhibiting good sorting and medium rounding and reflecting strong hydraulic characteristics.

Sand flat deposits in the central part of the study area, as observed in the Tupo profile (Figure 5e) and well TX 1 (Figure 4(e-1)) corresponding to the Yanghugou Formation, are characterized by the predominance of fine-grained sandstone to siltstone, displaying a vertically composite normal grading. The individual sand layers are relatively thin, approximately 0.2 to 0.5 m thick. The lower section exhibits the development of planar cross-bedding sandstone facies (Sp) and ripple cross-bedding siltstone facies (Fr), while the upper section is represented by flaser bedding siltstone facies (Fcf). This suggests a gradual decrease in tidal energy from the lower to upper portions of the sedimentary sequence. In terms of clastic components, the sandstone exhibits a relatively high silica content, fine grain size, moderate sorting, and medium to poor rounding, indicating a moderate to strong hydraulic energy.

Mixed flat deposits are primarily developed in the central part of the northern study area, where the Yanghugou Formation is intersected in well AC 1 (Figure 4(f-1)). It is dominated by siltstone–mudstone, exhibiting rhythmic interbedding of variable thicknesses of sand and mud. From the bottom to the top, the stratigraphic sequence changes from flaser bedding siltstone facies (Fcf) and wavy cross-bedding siltstone facies (Fcw) to lenticular bedding siltstone facies (Fcl). The upper section includes carbonaceous mudstone facies (Mc), with occasional occurrences of thin coal seam and coal line (C). Irregular rhombic bands of pyrite are observed in sandstone, indicating a weakly reducing environment [41]. Clastic components exhibit poor rounding and a high lithic content, reflecting the characteristics of sedimentation under relatively weak hydraulic energy.

4.2.3. Barrier-Island Lagoon

Barrier-island-lagoon sedimentary systems belong to barrier-coast sedimentary systems. Barrier islands are elongated sand ridges distributed parallelly to the coast, created by marine waves. They are characterized by a broad sea on the outer side and a lagoon on the inner side, separated from the mainland [42].

In the central part of the northern study area, typical developments of the barrier-island-lagoon sedimentary system are observed in the Xiaheyan profile (Figure 5g) and around well HT 1 (Figure 4(g-1)) where the Yanghugou Formation is recognized. The lithology of the barrier island is mainly composed of medium- to coarse-grained sandstone, exhibiting an overall inverse grading sequence. At the bottom of the stratigraphic sequence, there is ripple cross-bedding siltstone facies (Fr), transitioning upward to low-angle cross-bedding fine sandstone, parallel-laminated sandstone facies (Sh), and swash cross-bedding sandstone facies (Sl). At the top, fine conglomerates can be observed, with gravel particles having a diameter of approximately 1–2 cm, showing good sorting, indicative of a high-energy wave environment. The extensive sandstone abruptly changes upward to horizontal bedding mudstone facies (Mh), where mudstone contains numerous pyrite nodules and siderite nodules. Locally, massive marl facies (Lm) and thin coal seams (C) less than 1 m thick can be seen, representing the sedimentary characteristics of the lagoon behind the barrier island. The clastic components are predominantly quartz, showing good particle sorting and rounding, indicating multiple episodes of seawater scouring. The lagoon lithology is dominated by mudstone, containing fragments of aquatic and plant fossils. Sedimentary structures are primarily characterized by horizontal laminations, reflecting relatively weak hydraulic conditions.

4.2.4. Continental Shelf

Continental shelf sedimentation occurs in extensive shallow sea areas near the wave base, generally extending from the low-tide line to approximately 70 m under water [6]. In the central part of the study area, typical developments of continental shelf sedimentation are observed in the Dashitoujingou profile (Figure 5h) and well Z6 (Figure 4(h-1)) where the middle section of the Yanghugou Formation was recognized. Below the wave base, the water energy is low, so lithology is mainly composed of black mudstone, fine gray sandstone, and bioclastic mudstone. The sediment thickness of the section is greater than 50 m, with the development of horizontal bedding mudstone facies (Mh) at the bottom of the stratigraphic sequence, transitioning upward to ripple cross-bedding siltstone facies (Fr) indicative of wave influence, and the upper section is characterized by horizontal bedding mudstone facies (Mh).

The clastic components are primarily composed of quartz particles, well cemented and exhibiting good rounding. Clearly visible is the phenomenon of secondary enlargement of quartz, indicating the characteristics of reworked quartz. It is speculated that the quartz comes from sedimentary rock sources, and the transport distance is relatively long.

4.3. Paleocurrent Directions

The primary sedimentary structures reflecting palaeocurrent directions in the Yanghugou Formation clastic rocks are foreset laminae, whose trend indicates the direction of traction flow. Paleocurrent direction rose diagrams were marked on corresponding section points (Figure 6).

During the Yanghugou Formation deposition, the paleocurrent direction in the northern part of the study area was variable, primarily trending toward the northeast, northwest, and southwest directions. This reflects the interaction between the northern source regions such as the Alxa Block and Yanshan Ancient Land, as well as the influence of tidal action. In the southern part of the study area, the paleocurrent direction in the Dashitoujingou profile indicates a southerly direction, suggesting a predominant influence from the northern source regions. The paleocurrent direction in the Xiaheyan profile is primarily oriented in the east–west direction, indicating that the sand bodies were subjected to repeated disturbances due to wave action.

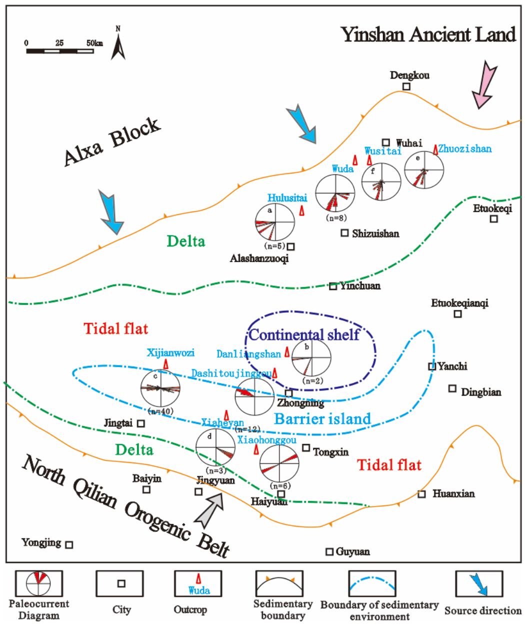

Figure 6. Rose chart of palaeocurrent measured in Yanghugou Formation, western of the Ordos Basin. Data in rose diagrams a,b,c, and d are from [33]; data in rose diagrams e and f are from [43].

5. U–Pb Geochronology of Detrital Zircon Grains

In total, 590 zircon U–Pb isotopic analyses were obtained from six sandstone samples (Table S1). Sample WD was collected from the Wuda profile. Sample HLST came from the Hulusitai profile. The samples DSTJG, SBT, SYK, and XHY were from the Dashitoujinggou, the Shabatai, the Suyukou, and the Xiaheyan profiles. The CL images of representative zircons and their U–Pb ages extracted from all samples are shown in Figure 5. The grain lengths range from 100 to 200 µm. The CL images show that most zircons maintained oscillatory or sector zonation (Figure 7). The Th/U ratio of the zircon grains ranges from 0.01 to 2.66. Most plot above the Th/U = 0.1 line (Figure 8), which usually reflects a magmatic origin [44,45].

We randomly selected 116 zircons from the sample WD, of which 112 grains were concordant. The concordant ages can be classified into four age groups: ca. 2534–2353 Ma, 2057–1707 Ma, 1380–742 Ma, and 528–301 Ma. In the probability density diagram (Figure 9), these analyses yield four age peaks at ca. 2446, 1940, 1090, and 457 Ma, respectively.

The SBT sample predominantly includes one strong age peaks at ca. 1897 Ma and three weak age peaks at ca. 443 Ma, 1335 Ma, and 2452 Ma. A total of 91 detrital zircons from sample HLST were used to produce the probability plot. The three major age peaks are at ca. 2413 Ma, 1846 Ma, and 317 Ma, respectively. In addition, there is a small number of zircon grains dated from ca. 1600 Ma to 600 Ma. Detrital zircons from sample SYK define only two dominant age peaks at ca. 2477 Ma and 2050 Ma. The DSTJG sample predominantly includes two strong age peaks at ca. 2431 Ma and 1990 Ma, which is similar to the relative probability diagrams of the SYK sample. The detrital zircons from sample XHY yield two major peaks at ca. 948 Ma and 443 Ma and show subordinate age groups at ca. 1876–1135 Ma and 813–649 Ma.

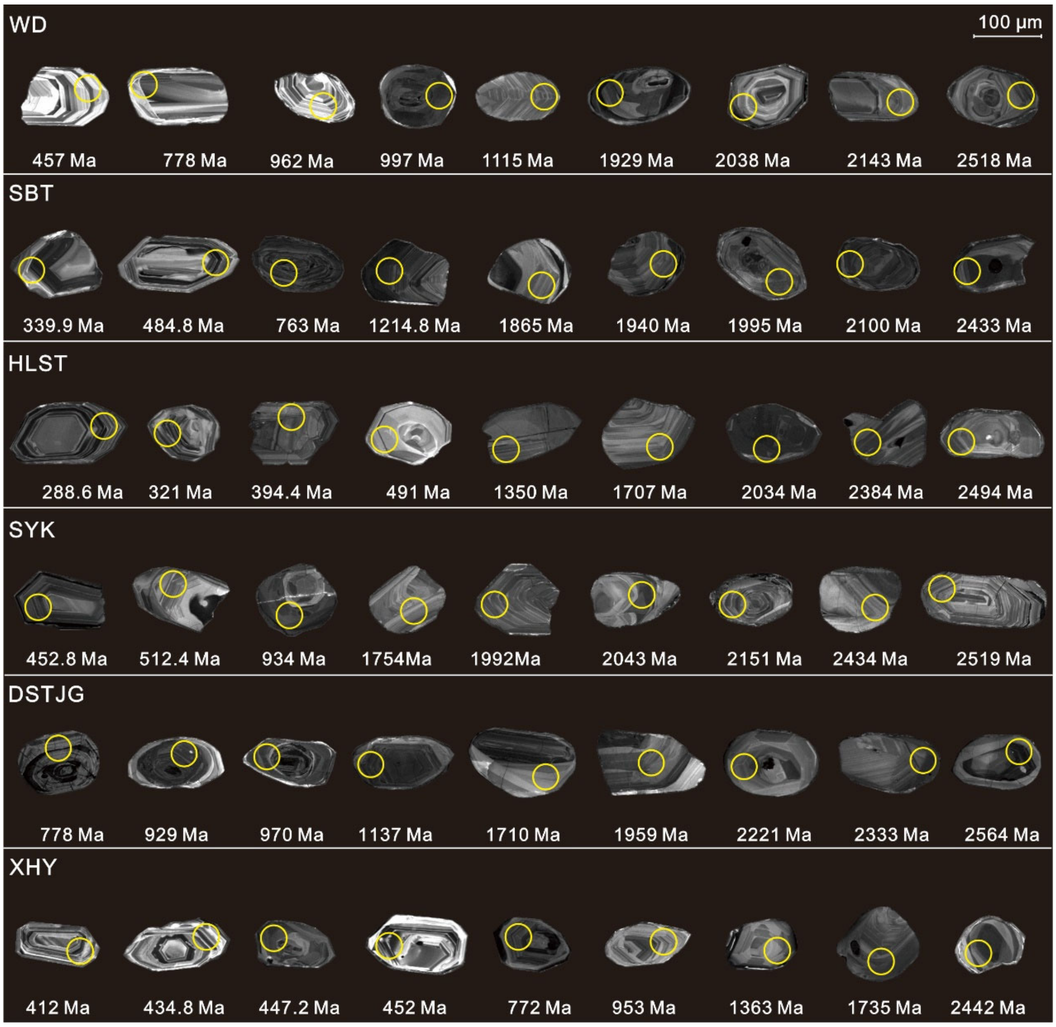

Figure 7. Representative CL images and U–Pb ages of detrital zircons from the six samples showing variations in size and morphology. The circles are analytical spots with a diameter of 33 μm.

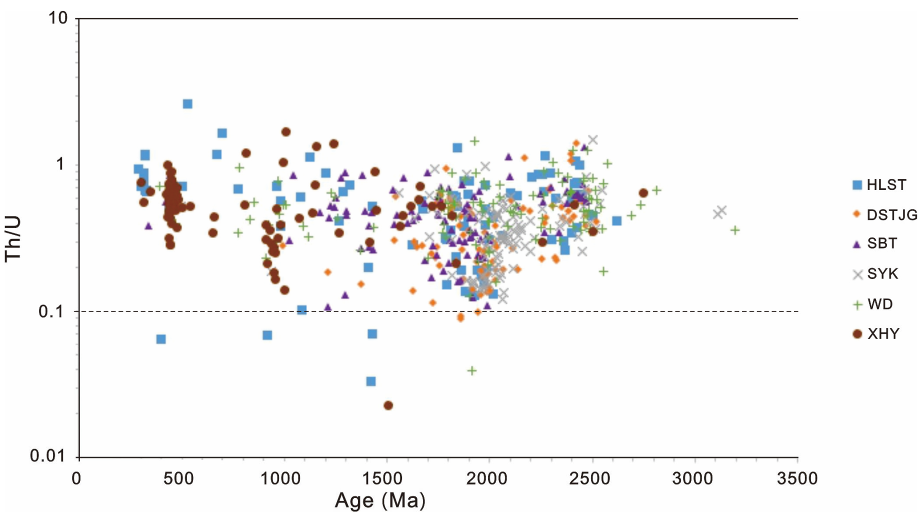

Figure 8. The distribution of zircon U–Pb ages vs. Th/U ratio of detrital zircons in the Upper Carboniferous Yanghugou Formation sandstone in western margin of the Ordos Basin.

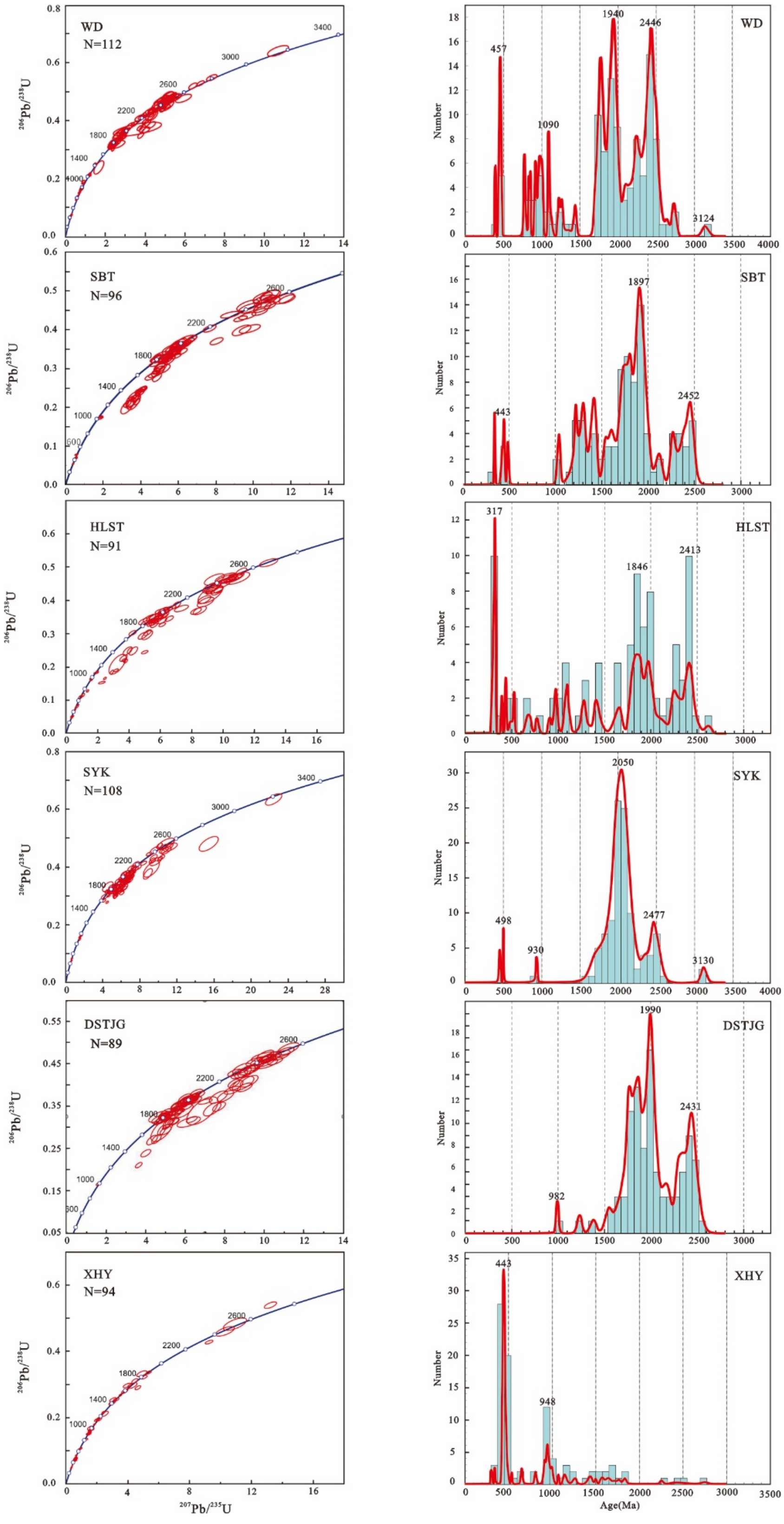

Figure 9. Concordia diagrams and relative probability diagrams showing detrital zircon U–Pb ages in the sandstone of the Yanghugou Formation. The red circles are zircon U-Pb ages reflecting the age error. The red lines are the probability den-sity curve of zircon U-Pb age distribution.

6. Detrital Zircon Trace Elements

In the chondrite-normalized REE diagram, most of the zircon grains show similar REE distribution patterns. The ∑HREE/∑LREE ratios of the samples are 10.76–442.04, with an average of 71.68, thus demonstrating enrichment of HREEs (Table S2). Most of the zircon grains show positive Ce anomalies (Ce/Ce* = 0.75–1741.60, with an average of 59.02) and negative Eu anomalies (Eu/Eu* = 0.02–1.24, with an average of 0.38) (Figure 10), typical of magmatic zircons [45].

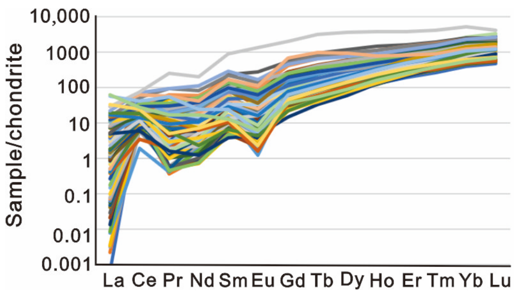

Figure 10. Chondrite-normalized REE patterns of all analyzed zircons in the sandstone of the Yanghugou Formation from the western margin of the Ordos Basin.

7. Discussion

7.1. Provenance of Detrital Zircon Grains

The zircon concordant U–Pb age spectra for 590 representative detrital zircon grains from the Yanghugou Formation on the western margin of the Ordos Basin reveal five distinct populations (Figure 9): (1) ca. 2600–2200 Ma; (2) ca. 2000–1800 Ma; (3) ca. 1600–1000 Ma; (4) ca. 1000–550 Ma; and (5) ca. 500–300 Ma.

The oldest age population at ca. 2600–2200 Ma corresponds to the tectonic thermal events of the Yinshan Orogenic Block and Alxa Block in the North China Craton (NCC) during the Neoarchean–Paleoproterozoic interval (Figure 11) [46,47]. The formation ages of the original rocks in the Yinshan Oldland, including the greenstone belts, granitic intrusions, and high-grade metamorphic complexes, are mainly ca. 2560 to 2510 Ma, at the end of the Neoarchean period [48]. The Alxa Block contains a gneiss basement of ca. 2400–2200 Ma. All samples in the study area except for XHY showed this age population.

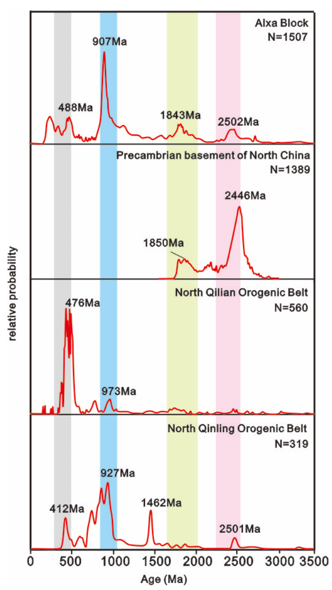

Figure 11. Zircon U–Pb age spectra of potential sediment sources. The age distribution curves on the Alxa Block and North Qilian Orogenic Belt are modified from Zhao et al. [33], while those for the Precambrian

basement of North China are from Zhou et al. [49] and those for the North Qinling Orogenic Belt are from Shi et al. [50] and the references therein. The gray in image represents the age at ca. 300–500 Ma. The blue represents the age at ca. 800–1000 Ma. The yellow represents the age at ca. 1800–2000 Ma. The pink represents the age at ca. 2200–2600 Ma

The second age population at ca. 2000–1800 Ma (with a peak of approximately ca. 1900 Ma) is found in five samples except for XHY. The discovery of two ancient Himalayan-type collisional orogenic belts (ca. 1950 Ma Khondalite Belt in the western part of the NCC and ca. 1850 Ma Trans-North China Orogen in the central part) confirmed that the basement of the NCC resulted from the amalgamation of several microcontinental blocks at ca. 1950 Ma and ca. 1850 Ma, recording assembly of the Columbia supercontinent [46,51–55].

The Middle Proterozoic ca. 1600–1000 Ma age population is visible in the WD, SBT, and HLST. The zircon dating of the gneissic granite in the Yaoquan area of Ayou Banner in the Alxa Block shows an age of ca. 1269 $\pm$ 90 Ma [56], and the U–Pb age of the zircon in the Hongaobao plagioclase granite body is ca. 1256 Ma [57], which may reflect a significant tectonic thermal event that occurred in the Alxa Block during this period [56]. The NCC lacks this tectonic thermal event.

The age population in the range of the Neoproterozoic (ca. 1000 to 550 Ma) is found in samples WD and HLST. This age population is absent in the NCC, but there is a large number of magmatic records in the Alxa Block at that time (Figure 11) [33].

The age population at ca. 500–300 Ma is found in five samples except the DSTJG. This population represents magmatic activity in the initial stage of the Caledonian Movement (ca. 400–500 Ma) and is best explained as being related to the subduction of the Qilian Block toward the Alxa Block [58,59]. The Carboniferous (ca. 350–320 Ma) magmatic rocks of the Longshou Mountains, Beida Mountains, Bayanwula Mountains, and Honggueryulin and Langshan areas in the Alxa Block mainly include intermediate acid adakitic intrusive rocks and a few mafic rocks.

The trace element data of zircon can distinguish between I-type and S-type granite protoliths [60]. The average phosphorus (P) content in S-type granite zircons is greater than in I-types. In this study, the trace elements of zircons in the study area were grouped according to the age and analyzed (Figure 12). The five samples in the study area, except for XHY, contain a large amount of both I-type and S-type Archean Paleoproterozoic zircons, which are speculated to be related to the late Archean I-type and S-type granites in the northern part of the study area. For example, the late Archean granite diorite type in the Langshan area in the northern part of the study area belongs to I-type granite [61]. The Archean I-type granite type is distributed in the Qianhao area of the middle section of the Daqingshan area [62]. The ca. 1.95 Ga S-type granite is exposed in the northern section of the Helan Mountain in the northwest of the study area [63]. There are ca. 1.88–1.86 Ga S-type granite intrusion events in the Helan and Qianlishan areas [52,64]. Sandstone samples from Shabatai contain a significant amount of Middle Proterozoic zircons, predominantly of S-type. It is speculated that these zircons may originate from the Red Aobao S-type diorite in the Yabulai-Bayan Nurian public structural belt [56]. XHY samples exhibit distinct I-type Early Paleozoic zircons, corresponding to the widespread Paleozoic I-type granites in the North Qilian Orogenic Belt and North Qinling Orogenic Belt located in the southwestern part of the study area [65,66].

Based on the characteristics of the zircon age spectrum and zircon classification results, it is inferred that the materials of the Shabatai, Wuda, and Hulusitai sections are mainly provided by the Alxa Block and the Yinshan Ancient Land, while the materials of the Suyukou and Dashishiujinggou sections mainly come from the Yinshan Ancient Land, and the materials of the Xiaheyan sections mainly come from the North Qilian or North Qinling Orogenic Belts. However, considering the scarcity of zircons from the Neoproterozoic era in the Xiaheyuan section and their difference from the zircon U–Pb age spectra of the North Qinling Orogenic Belt, it is deduced that Xiaheyuan primarily receives materials from the North Qilian Orogenic Belt.

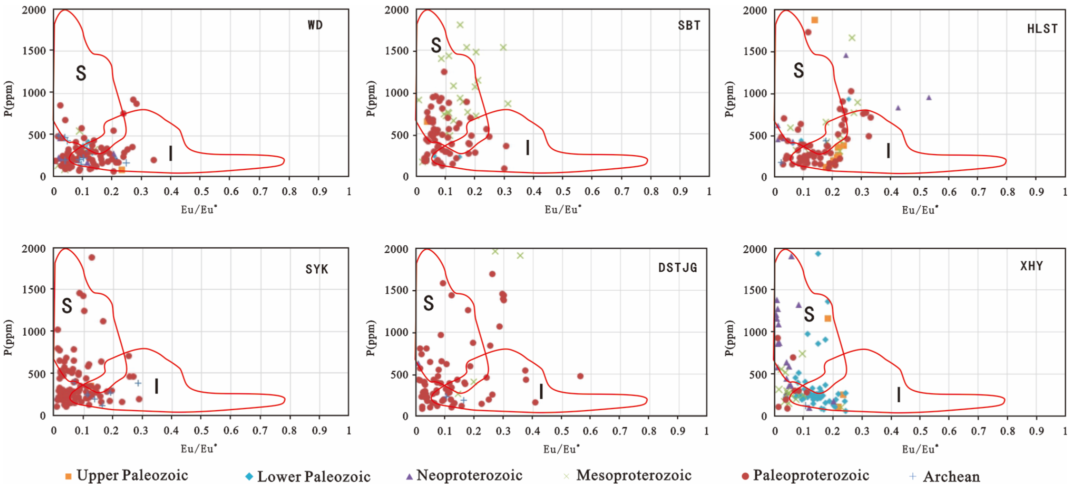

Figure 12. Scatter plot of the I- and S-type zircons in the diagrams of the P content versus Eu anomaly [67].

7.2. Characteristics of Source–Sink Regions

For a better understanding of the source–sink system of the Yanghugou Formation in the western edge of the Ordos Basin, we synthetically presented the age populations of 14 sandstone samples (combined with 8 samples from previous studies) in the study area (Figure 13). On the basis of the U–Pb age heterogeneity and sample localities, we divided the study area into four sub-regions.

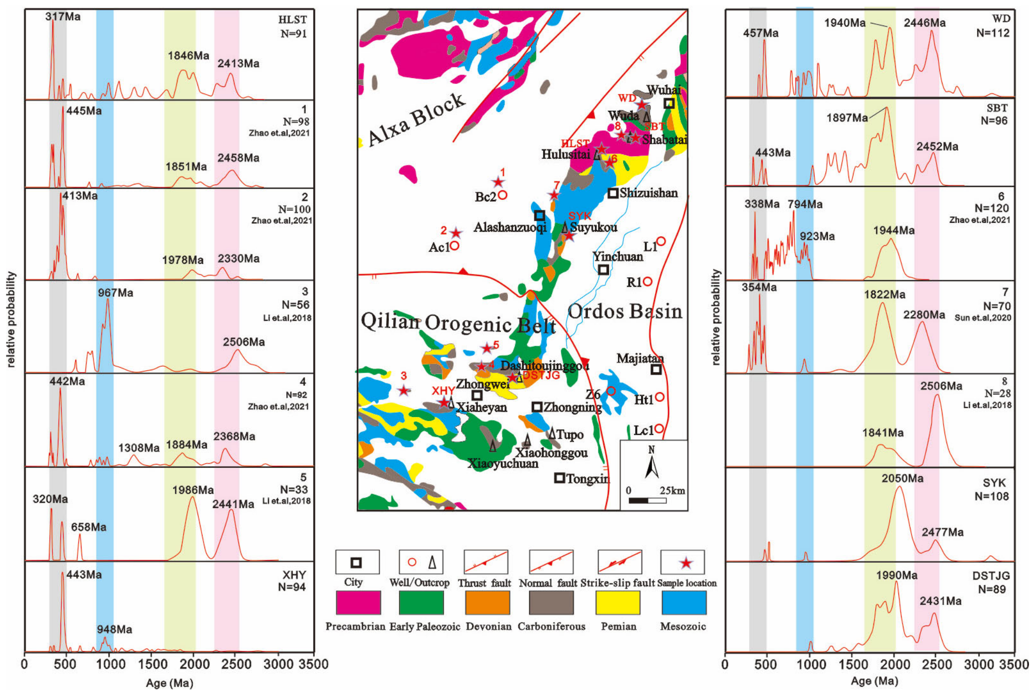

Figure 13. Diagram showing age distributions of detrital zircons from the Yanghugou Formation in the western Ordos Basin [33,43,68]. The gray in image represents the age at ca. 300–00 Ma. The blue represents the age at ca. 800–1000 Ma. The yellow represents the age at ca. 1800–2000 Ma. The pink represents the age at ca. 2200–2600 Ma.

7.2.1. Alxa Source–Sink Region

This source–sink region encompasses the eastern part of the Alxa Block, extending from the BC 2 well to the south, covering the areas of Hulustai to the west of Zhongwei (Figure 14). The strata of the Yanghugou Formation in this region exhibit detrital zircon

U–Pb age spectra with two predominant age groups: ca. 1000–800 Ma and 500–320 Ma, along with two minor age groups: ca. 2600–2200 Ma and 2000–1800 Ma (Figure 13). The results indicate that the region can be further subdivided into two sub-areas based on age. One sub-area comprises four samples characterized by detrital zircons from the ca. 500–320 Ma age group. Another sub-area is dominated by detrital zircons from the ca. 1000–800 Ma age group, which is quite different from the age compositions of the other four samples in this region.

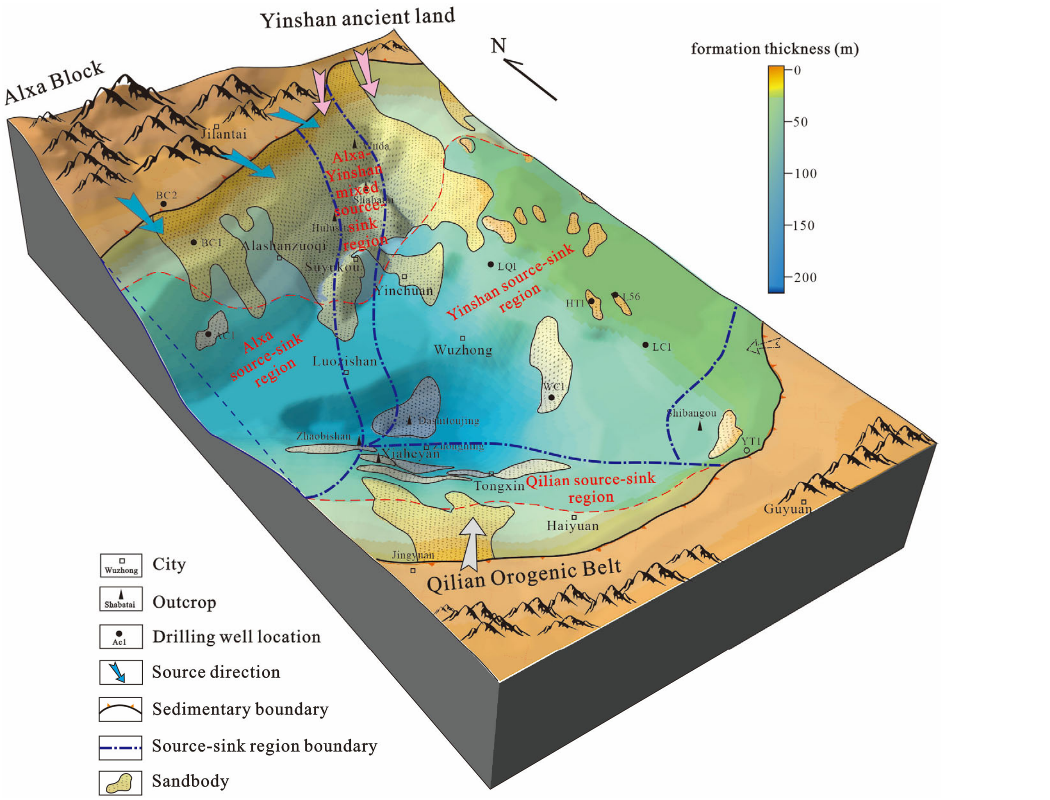

Figure 14. Paleogeographic map of the Yanghugou Formation in the western margin of the Ordos Basin.

7.2.2. Yinshan Source–Sink Region

This source–sink area includes the Yinshan Ancient Land—Suyukou—Dashiujinggou Line to the east (Figure 14). The strata of the Yanghugou Formation in this area show detrital zircon U–Pb age spectra characterized by the typical presence of age populations at ca. 2600–2200 Ma and 2000–1800 Ma (Figure 13). Zircons of other ages are almost absent, indicating that this area is solely sourced from the Yinshan Ancient Land.

7.2.3. Alxa–Yinshan Mixed Source–Sink Region

Located in the Alxa–Yinshan–Wuda–Zhaobishan region (Figure 14), this source–sink area exhibits detrital zircon U–Pb age spectra dominated by three age groups: ca. 2600–2200 Ma, 2000–1800 Ma, and 500–320 Ma (Figure 13). This suggests that the zircons in this area originate from both the Yinshan Ancient Land and the Alxa Block.

7.2.4. Qilian Source–Sink Region

The term refers to the region extending southeastward from the Qilian Mountains directly to the Xiaheyan section (Figure 14). In this area, the strata of the Yanghugou Formation exhibit detrital zircon U–Pb age spectra characterized by a prominent age population at ca. 500–400 Ma (Figure 13). Notably, zircons from the Paleoproterozoic to the Archean are essentially absent, excluding contributions from the Yinshan Ancient Land and the Alxa Block.

Referring to previous studies on the sandstone mineralogy in the research area [18], it is speculated that materials from the northern Qinling may be present near Shibangou in the southeastern part of the study area. However, due to the limited data in this study, we do not discuss this further.

7.3. Paleogeographic Patterns

Based on the characteristics of sedimentary facies, zircon geochronology, and palaeocurrent analysis in the study area, we reconstructed the filling process and paleogeographic patterns of the Yanghugou Formation on the western margin of the Ordos Basin (Figure 14). Overall, the deposition period of the Yanghugou Formation represents a transitional environment between marine and continental settings, undergoing processes of water deepening and shallowing.

In the northwestern part of the study area, the clastic sediments are primarily sourced from the stable Alxa Block. Exposed and eroded rocks include Paleoproterozoic to Mesoproterozoic schist, marble, crystalline schist [69–72], Granite Syenite formed by the subduction of the early Paleozoic North Qilian oceanic crust beneath the Alxa Block [73], and Granite Porphyry influenced by the tectonic evolution of the Late Paleozoic Central Asian Orogenic Belt [74]. Combining palaeocurrent data, the sedimentary sand bodies supplied by the Alxa Ancient Land entered the northwestern part of the study area, originating as an active continental margin and continental island arc. The Alxa source–sink system's sedimentary sand bodies mainly consist of light gray to white pebbly quartz sandstone and lithic quartz sandstone, with high compositional maturity and moderate to good sorting and rounding. The sedimentary sand bodies extend a considerable distance, forming a fan-shaped progradation extending to the area south of Yinchuan. Features such as erosional surfaces at the base of sandstone, channelized cross-stratification, tabular cross-stratification, and occasional tidal laminations are common, indicating the sedimentary characteristics of a delta-barrier-island system in a strong water dynamic environment during the marine–continental transition.

In the northeastern part of the study area, clastic sediments primarily originate from the Yinshan Ancient Land. During the Late Paleozoic, the continuous southward subduction and closure of the Paleo-Asian Ocean led to the uplift of the Yinshan Ancient Land, serving as a source for sediments of the Yanghugou Formation [42]. Sediments supplied by the erosion of the Yinshan Ancient Land are transported in a northeast to southwest direction. The predominant lithologies include Proterozoic granite gneiss and Paleoproterozoic granite intrusions [75]. The Yinshan source–sink system's sedimentation is dominated by medium- to fine-grained lithic quartz sandstone, with interbedded gray-black mudstone bands. The sandstone exhibits high compositional maturity, moderate sorting, and the development of channelized cross-stratification and tabular cross-stratification. Some feather-like cross-stratification and tidal laminae suggest the influence of both fluvial and tidal processes, indicating a tidal-controlled delta-tidal-flat sedimentary system in a marine–continental transitional environment. In the vicinity of Dashitoujingou, the sediment thickness increases, and mudstone sediment increases, indicating a significant deepening of the sedimentary water body. The northern part of the Yinshan source–sink region has developed a tidal-controlled delta-tidal-flat sedimentary system in a marine–continental transitional environment, while the southern deep-water area has developed a shallow marine to semi-deep marine shelf sedimentary systems.

In the northern part of the study area, the clastic materials were mainly derived from the Alxa Block and the Yinshan Ancient Land in a mixed source region, transported from north to south. Due to active tectonics in the northern region, the Alxa Block and the Yinshan Ancient Land continuously supplied terrigenous clasts southward. The clastic sediments in this region are dominated by medium-grained lithic quartz sandstone and quartz sandstone, displaying features such as channelized cross-stratification, tabular cross-stratification, scouring surfaces, and feather-like cross-stratification. This suggests the development of a tidal-controlled delta-tidal-flat barrier-island sedimentary system in a marine–continental transitional environment.

In the southern part of the study area, sediments were mainly sourced from the Qilian Orogenic Belt, characterized by a tectonic setting dominated by a passive continental margin and, and in some areas, a continental island arc. The materials primarily originated from the Neoproterozoic crystalline basement of the Qilian Orogenic Belt [76] and Early Paleozoic magmatic rocks related to the subduction of the Qilian Ocean during the early Caledonian period and the collision between the Qilian and Alxa plates [22]. The clastic sediments entered the study area from the southwest and are dominated by quartz sandstone and feldspathic quartz sandstone. These sediments contain volcanic clastic deposits with altered volcanic fragments, suggesting a source from the Qilian Orogenic Belt. In the southern region, the sedimentary sand bodies are mainly composed of feldspathic quartz sandstone with moderate to low compositional maturity. These sediments are short-transported, reflecting a steep terrain slope and indicating near-source deposition. Nearshore sediment bodies exhibit small-scale fan-shaped progradation. In the Xiaheyan profile of Zhongwei, the sediments are characterized by coarse grain size, high quartz content, good sorting, and visible ripple marks and scouring cross-stratification, indicating a predominantly shoreface deposition with strong hydraulic conditions. The sedimentary characteristics indicate the development of small-scale deltas and barrier-island systems (Figure 14).

In the southeastern part of the study area, the Central Paleouplift was relatively gentle and low during the early deposition of the Yanghugou Formation but experienced gradual submergence due to the connection between the North China Sea and the Qilian Sea later in the depositional period. It became an underwater paleouplift, unable to completely block the supply of source materials and the transport of sediments within the basin [77]. The area above the underwater paleouplift is dominated by tidal flat deposits.

7.4. Relationship between the North China Craton and the Alxa Block

Previous studies have extensively discovered Middle Proterozoic gneissic granite [56], Neoproterozoic granite [78–80], and a series of magmatic activity records in the early Paleozoic extensional environment of the Alxa Block [58,59]. However, structurally adjacent to the western part of the North China Craton, there are no contemporaneous magmatic thermal events, nor are there sources from the Alxa Block [81]. Therefore, it is inferred that before the Early Paleozoic, the NCC, and the Alxa Block were separated.

Through the exploration of the provenance and paleogeography of the Yanghugou Formation in the western margin of the Ordos Basin, it is concluded that there were materials sourced from the Alxa Block in both the Alxa source–sink region in the northwestern part and the Alxa–Yinshan mixed source–sink region in the northern part. Therefore, we infer that the amalgamation of the Alxa Block and the NCC should have been completed before the late Carboniferous.

7.5. Exploration Potential Analysis

The parent rock type, transport distance, sand body thickness, and sedimentary facies in different source–sink regions will affect the reservoir's physical properties and then affect the exploration potential. The parent rock provides the material basis of sandstone reservoir components. The parent rocks of the Alxa source–sink region are mainly alkaline basalt and granite; the parent rocks of the Yinshan source–sink region are mainly calcareous argillaceous sedimentary rocks and granite, and the parent rocks of the Qilian source–sink region are mainly calcareous argillaceous sedimentary rocks [18]. The sand body in the northwest has a high quartz content [18], so it has a strong anti-compaction effect. The genetic mechanism of sand bodies in different source–sink regions is different, and the physical properties are also different. The delta-front sand bodies in the study area show the best reservoir properties, followed by barrier sand bars, while the tidal flat and shelf sand bodies have poor reservoir properties [82]. In terms of sand body thickness, the sand body thickness in the Alxa source–sink region is 10–60 m, the sand body thickness in the Yinshan source–sink region is 30–90 m, the sand body thickness in the Alxa–Yinshan mixed source–sink region is 30–150 m, and the sand body thickness in the Qilian source–sink region is 20–80 m. In summary, the delta sand bodies in the Alxa–Yinshan mixed source–sink region have the best reservoir performance and have great exploration potential.

8. Conclusions

1. Based on the comprehensive analysis of detrital zircon U–Pb geochronology and geochemistry, palaeocurrent direction, lithofacies types, and sedimentary characteristics of the Upper Carboniferous Yanghugou siliciclastic sequences, four main source–sink regions are recognized: the Alxa, Yinshan, Alxa–Yinshan, and Qilian.
2. In the Alxa source–sink region, transitional delta-barrier-island sediments are developed, with quartz sandstone and lithic quartz sandstone as the main sandstones with high compositional maturity. The northern part of the Yinshan source sink region develops a coastal-transitional tidal-controlled delta-tidal-flat sedimentary system, with a deepwater area characterized by shallow marine to semi-deep marine shelf sedimentary systems. The sandstone in the Yinshan source–sink region has a long transportation distance and the highest compositional maturity, mainly composed of quartz sandstone. The Alxa–Yinshan mixed source–sink region has developed a tidal-controlled delta-tidal-flat barrier-island sedimentary system, with high compositional and structural maturity of sandstone. The Qilian source–sink region has developed small-delta and barrier-island sedimentary systems, with low compositional maturity of sandstone.
3. The Alxa source–sink region and the Alxa–Yinshan mixed source–sink region both contain materials from the Alxa Block. Therefore, from the perspective of a source–sink system analysis, it is inferred that the Alxa Block had already merged with the North China Craton before the Late Carboniferous Yanghugou Formation.
4. The delta sand bodies in the Alxa–Yinshan mixed source–sink region have the best reservoir performance and have great exploration potential.

Supplementary Materials: The following supporting information can be downloaded at: https://www.mdpi.com/article/10.3390/min14010078/s1, Supplementary Table S1: Zircon LA-ICP-MS U-Pb isotope data from the Yanghugou Formation sandstones in western margin of the Ordos Basin. Supplementary Table S2: Zircon trace element data from the Yanghugou Formation sandstones in western margin of the Ordos Basin.

Author Contributions: Conceptualization, T.Z., R.C., F.W. and L.L.; formal analysis, T.Z.; investigation, T.Z., R.C. and F.W.; resources, J.H.; data curation, M.Z., Q.L. and J.W.; writing—original draft preparation, T.Z.; writing—review and editing, T.Z., R.C. and F.W.; supervision, R.C.; project administration, R.C.; funding acquisition, F.W. All authors have read and agreed to the published version of the manuscript.

Funding: This research was funded by the Changqing Oilfield Funded Project, grant number 2023DZZ02, 2020-JS-51586.

Data Availability Statement: Data is contained within the article and Supplementary Material.

Acknowledgments: Authors thank the editors and anonymous referees for their helpful comments. Analysis in the JdLC GeoHistory Laser Ablation Facility was enabled by the Research Office, Curtin, AuScope (auscope.org.au (accessed on 1 November 2023)) and the Australian Government via the National Collaborative Research Infrastructure Strategy (NCRIS). Brad McDonald and Noreen J. Evans are thanked for help with LA-ICP-MS setup.

Conflicts of Interest: Authors Tao Zhang and Jianling Hu are employed by the PetroChina Changqing Oilfield Company. The remaining authors declare that the research was conducted in the absence of any commercial or financial relationships that could be construed as a potential conflict of interest.

References

1. Yang, G.L.; Ren, Z.L.; He, F.Q.; Zhang, Y.Y.; Wang, B.J.; Qi, K. Fault-fracture body growth and hydrocarbon enrichment of the Zhenjing area, the southwestern margin of the Ordos Basin. *Oil Gas Geol.* **2022**, *43*, 1382–1396.
2. Deng, X.Q.; Fu, J.H.; Yao, J.L.; Pang, J.L.; Sun, B. Sedimentary facies of the Middle-Upper Triassic Yanchang Formation in Ordos Basin and breakthrough in petroleum exploration. *J. Palaeogeogr.* **2011**, *13*, 443–455.
3. Xi, S.L.; Huang, J.P.; Zhang, C.L.; Li, X.B.; Jing, X.H.; Lin, J.F.; Guo, W.; Zhang, Y. Discovery and Source Analysis of Oil Sands in the Yanghugou Formation of the Carboniferous in the Western Margin of the Ordos Basin. *Acta Geol. Sin.* **2022**, *96*, 1041–1052.
4. Fu, S.T.; Tian, J.C.; Chen, H.D.; Hou, J.Z.; Zhang, J.Q.; Liu, W.Y.; Yang, H.; Fu, J.H.; Fan, Z.P.; Shi, X.Y. The delta depositional system distribution of Late Paleozoic Era in Ordos Basin. *J. Chengdu Univ. Technol.* **2003**, *30*, 236–241.
5. Wang, C.J.; Xu, H.; Yang, G.; Cao, D.Y.; Xia, Y.Y. Geological conditions of Yanghugou formation shale gas accumulation on western margin of Ordos basin. *Cola Geol. China* **2014**, *26*, 18–24.
6. Tyson, R.V. Sedimentation rate, dilution, preservation and total organic carbon: Some results of a modelling study. *Org. Geochem.* **2001**, *32*, 333–339. [CrossRef]
7. Mansoura, A.; Wagreichb, M.; Gentzisc, T.; Ocubalidetc, S.; Tahound, S.S.; Elewaa, A.M.T. Depositional and organic carbon-controlled regimes during the Coniacian-Santonian event: First results from the southern Tethys (Egypt). *Mar. Pet. Geol.* **2020**, *115*, 1–18. [CrossRef]
8. Mansour, A.; Wagreich, M. Earth system changes during the cooling greenhouse phase of the Late Cretaceous: Coniacian-Santonian OAE3 subevents and fundamental variations in organic carbon deposition. *Earth-Sci. Rev.* **2022**, *229*, 1–35. [CrossRef]
9. Hou, Y.D.; Chen, A.Q.; Zhao, W.B.; Dong, G.D.; Yang, S.; Xu, S.L.; Gao, Z.D.; Li, F.X.; Liu, X.X.; Zhang, X.X. Analysis on the depositional environment of Carboniferous Benxi Formation tidal-delta sand body complex, Ordos Basin, China. *J. Chengdu Univ. Technol. Sci. Technol. Ed.* **2018**, *45*, 393–401.
10. Guo, Y.Q.; Wang, M.X.; Guo, B.C.; Cai, Z.C.; Hui, L.; He, Z.Q.; Ma, Y.; Li, W.H.; Li, B.Q. Sedimentary system characteristics and paleographic evolution of Upper Paleozoic of northern west margin, Ordos Basin. *J. Northwest Univ. Nat. Sci. Ed.* **2020**, *50*, 93–104.
11. Wei, J.Y.; Wang, H.W.; Liu, G.; Li, H.; Cao, Q. Sedimentary characteristics of the Yanghugou Formation of the Carboniferous in the western margin thrust belt of the Ordos Basin. *Lithol. Reserv.* **2023**, *35*, 120–130.
12. Feng, J.P.; Ouyang, Z.J.; Chen, Q.H.; Li, W.H. Sedimentary characteristics of the Upper Carboniferous in Ordos Basin and its adjacent areas. *J. Palaeogeogr. Chin. Ed.* **2021**, *23*, 53–64.
13. Si, J.; Hu, Y.; Hou, Y.D.; Sun, J.F.; He, W.X.; Lu, Y.S. Geochemical characteristics and paleoenvironmental significance of the Carboniferous Yanghugou Formation in the northern part of the western margin of Ordos Basin: A case study of the Wuda outcrop. *Sci. Technol. Eng.* **2021**, *21*, 11514–11526.
14. Wang, B.X.; Xu, G.F.; Guo, H.J.; Hao, Z.L.; He, W.X.; Hu, Y.; Hou, Y.D.; Sun, J.F. Palynological characteristics of Yanghugou Formation at western margin of Ordos Basin, NW China, and paleoclimatic implications. *Technol. Rev.* **2023**, *41*, 113–124.
15. Wang, J.; Wang, F.; Zhao, W.B.; Hu, J.L.; Wu, J.Y.; Xiao, Y.Y.; Chen, H.D.; Liu, L.; Wang, Z.W.; Zhu, S.Y. Lithofacies Types and Sedimentary Models of the Upper Carboniferous Yanghugou Formation in the Western Margin of the Ordos Basin. *J. Palaeogeogr.* **2023**, *25*, 573–597.
16. Chen, Q.H.; Li, W.H.; Liu, H.W.; Li, K.Y.; Pang, J.G.; Guo, Y.Q.; Yuan, Z. Provenance analysis of sandstone of the Upper Carboniferous to Middle Permian in Ordos Basin. *J. Palaeogeogr.* **2009**, *11*, 629–640.
17. Zhao, Q.P.; Wang, R.G.; Gao, F.; Yin, X. Provenance analysis of Upper Paleozoic in Yanchang Blocks, the southeast Ordos Basin. *J. Northwest Univ. Nat. Sci. Ed.* **2015**, *45*, 933–941.
18. Zhu, S.Y.; Liu, L.; Hu, J.L.; Chen, B.; Wang, Z.W.; Shi, Y.H.; Du, X.W.; Wang, F.; Chen, H.D.; Zhang, C.G.; et al. Characteristics of the Source-to-Sink System and Paleogeographical Pattern from the Upper Carboniferous Yanghugou Formation in Western Margin of the Ordos Basin. *Acta Sedimentol. Sin.* **2023**, *41*, 1430–1450.
19. Zuza, A.V.; Yin, A. Balkatach hypothesis: A new model for the evolution of the Pacific, Tethyan, and Paleo-Asian oceanic domains. *Geosphere* **2017**, *13*, 1664–1712. [CrossRef]
20. He, T.Y.; Liu, T.; Li, G. Geological structural features and exploration direction in the western margin of Ordos Basin. *Oil Geophys. Prospect.* **2005**, *40*, 65–69.
21. Wu, C.H.; Zhong, C.T. The Paleoproterozoic SW-NE collision model for the central North China Craton. *Prog. Precambrian Res.* **1998**, *21*, 28–50.
22. Song, S.G.; Niu, Y.L.; Su, L.; Xia, X.H. Tectonics of the North Qilian orogeny, NW China. *Gondwana Res.* **2013**, *23*, 1378–1401. [CrossRef]
23. Zhou, L.R.; Yu, P.S. Isotopic ages and their geologic significance of AB. *Northwest. Geol.* **1989**, *1*, 52–63.
24. Li, B.; Meng, Z.F.; Xia, B.; Lu, H.X.; Zheng, M. Tectonic Evolution Characteristics of the Western Margin of the Ordos Basin. *Northwest Oil Gas Explor.* **2006**, *18*, 29–34.
25. Zhao, Y.; Zhai, M.G.; Chen, H.; Zhang, S.H. Paleozoic-Early Jurassic tectonic evolution of North China Craton and its adjacent orogenic belt. *Geol. China* **2017**, *44*, 44–60.
26. Zhang, G.W.; Zhang, Z.Q.; Dong, Y.P. Nature of main tectono-lithostratigraphic units of the Qinglin orogen: Implications for the tectonic evolution. *Acta Pelrologica Sin.* **1995**, *11*, 101–114.
27. Zhao, C.Y.; Liu, C.Y. *Formation and Evolution of the North China Cratonic Sedimentary Basin and Its Hvdrocarl on Occurrence*; Northwest University Publishing Press: Xi'an, China, 1990; pp. 1–189.

28. Yan, C.F.; Yuan, J.Y.; Zhao, Y.C. Carboniferous lithofacies paleogeography in eastern North Qilian. *Acta Sedimentol. Snica* **2008**, *26*, 193–201.
29. Zhao, Z.Y.; Liu, C.Y. *Formation and Evolution of Sedimentary Basins in North China Craton and Their Oil and Gas Occurrence*; Northwest University Publishing Press: Xi'an, China, 1990.
30. Zhai, Y.H.; He, D.F.; Ma, J.H.; Kai, B.Z.; Cheng, X.; Xu, Y.H. Tectonic-depositional environment and prototype basins during the depositional period of Late Carboniferous Benxi Formation in Ordos Basin. *Chin. J. Geol.* **2020**, *55*, 726–741.
31. Shen, B.H.; Shen, S.Z.; Wu, Q.; Zhang, S.C.; Zhang, B.; Wang, X.D.; Hou, Z.S.; Yuan, D.X.; Zhang, Y.C.; Liu, F.; et al. Carboniferous and Permian integrative stratigraphy and timescale of North China Block. Sci. *China Earth Sci.* **2022**, *65*, 983–1011. [CrossRef]
32. Haq, B.U.; Schutter, S.R. A chronology of Paleozoic sea-level changes. *Science* **2008**, *322*, 64–68. [CrossRef]
33. Zhao, J.F.; Zhou, Y.; Wang, K.; Li, X.; Ma, Z.; Ruan, Z.Z.; Wang, D.; Xue, R. Provenance and paleogeography of carboniferous-permian strata in the bayanhot basin:constraints from sedimentary records and detrital zircon geochronology. *Geosci. Front.* **2021**, *12*, 101088. [CrossRef]
34. Barham, M.; Reynolds, S.; Kirkland, C.L.; O'Leary, M.J.; Evans, N.J.; Allen, H.J.; Haines, P.W.; Hocking, R.M.; McDonald, B.J. Sediment routing and basin evolution in Proterozoic to Mesozoic east Gondwana: A case study from southern Australia. *Gondwana Res.* **2018**, *58*, 122–140. [CrossRef]
35. Chen, R.; Wang, F.; Li, Z.; Evans, N.J.; Chen, H.D. Detrital zircon geochronology of the Permian Lower Shihezi Formation, northern Ordos Basin, China: Time constraints for closing of the Palaeo-Asian Ocean. *Geol. Mag.* **2022**, *159*, 1601–1620. [CrossRef]
36. Stern, R.A.; Bodorkos, S.; Kamo, S.L.; Hickman, A.H.; Corfu, F. Measurement of SIMS Instrumental Mass Fractionation of Pb Isotopes During Zircon Dating. *Geostand. Geoanalytical Res.* **2009**, *33*, 145–168. [CrossRef]
37. Spencer, C.J.; Kirkland, C.L.; Taylor, R.J.M. Strategies towards statistically robust interpretations of in situ U-Pb zircon geochronology. *Geosci. Front.* **2016**, *7*, 581–589. [CrossRef]
38. Miall, A.D. Architectural-element analysis: A new method of facies analysis applied to fluvial deposits. *Earth Sci. Rev.* **1985**, *22*, 261–308. [CrossRef]
39. Jia, J.H. Sedimentary microfacies and sandbody distribution in the clastic tidal environment of the ancient coastal zone: A case study of Silurian in Tazhong area, Tarim basin. *J. China Univ. Min. Technol.* **2019**, *48*, 110–123.
40. Longhitano, S.G.; Mellere, D.; Steel, R.J.; Ainsworth, R.B. Tidal depositional systems in the rock record: A review and new insights. *Sediment. Geol.* **2012**, *279*, 2–22. [CrossRef]
41. Jing, Z.K.; Wang, J.Y.; Liang, T.; Zhu, X.E.; Yu, K.H.; Su, N.N.; Zhao, J.H.; Guo, S.H.; Chen, H.; Jiao, P.P.; et al. *Sedimentary Geology*; Petroleum Industry Press: Beijing, China, 2021.
42. Wang, G.R. *The Study of Sources and Senquence-Lithofaces Palaeogeography of Upper Palaeozoic, Northern Ordos*; Chengdu University of Technology: Chengdu, China, 2011.
43. Sun, J.P.; Dong, Y.P. Stratigraphy and geochronology of Permo-Carboniferous strata in the western North China Craton: Insights into the tectonic evolution of the southern Paleo-Asian Ocean. *Gondwana Res.* **2020**, *88*, 201–219. [CrossRef]
44. Williams, I.S.; Claesson, S. Isotopic evidence for the Precambrian provenance and Caledonian metamorphism of high-grade paragneiss from the Seve Nappes, Scandinavian Caledonides. *Contrib. Mineral. Petrol.* **1987**, *97*, 205–217. [CrossRef]
45. Hoskin, P.W.O.; Ireland, T.R. Rare earth element chemistry of zircon and its use as a provenance indicator. *Geology* **2000**, *28*, 627–630. [CrossRef]
46. Wan, Y.S.; Liu, D.Y.; Dong, C.Y.; Xu, Z.Y.; Wang, Z.J.; Wilde, S.A.; Liu, Z.H.; Yang, Z.S.; Zhou, H.Y. The Precambrian Khondalite Belt in the Daqingshan area, North China Craton: Evidence for multiple metamorphic events in the Palaeoproterozoic. *Geol. Soc. Spec. Publ.* **2009**, *323*, 73–97. [CrossRef]
47. Jian, P.; Kröner, A.; Windley, B.F.; Zhang, Q.; Zhang, W.; Zhang, L.Q. Episodic mantle melting-crustal reworking in the Late Neoarchean of the northwestern North China Craton: Zircon ages of magmatic and metamorphic rocks from the Yinshan Block. *Precambrian Res.* **2012**, *222–223*, 230–254. [CrossRef]
48. Zhang, J.X.; Gong, J.H. Revisiting the nature and affinity of the Alxa Block. *Acta Petrol. Sin.* **2018**, *34*, 940–962.
49. Zhou, W.Y.; Jiao, Y.Q.; Zhao, J.H. Sediment Provenance of the Intracontinental Ordos Basin in North China Craton Controlled by Tectonic Evolution of the Basin-Orogen System. *J. Geol.* **2017**, *125*, 701–711. [CrossRef]
50. Shi, Y.; Yu, J.H.; Santosh, M. Tectonic evolution of the Qinling orogenic belt, Central China: New evidence from geochemical, zircon U-Pb geochronology and Hf isotopes. *Precambrian Res.* **2013**, *231*, 19–60. [CrossRef]
51. Wilde, S.A.; Zhao, G.C.; Sun, M. Development of the North China Craton during the Late Archaean and its final amalgamation at 1.8 Ga: Some speculations on its position within a global palaeoproterozoic supercontinent. *Gondwana Res.* **2002**, *5*, 85–95. [CrossRef]
52. Yin, C.Q.; Zhao, G.C.; Guo, J.H.; Sun, M.; Xia, X.P.; Zhou, X.W.; Liu, C.H. U-Pb and Hf isotopic study of zircons of the Helanshan Complex: Constrains on the evolution of the Khondalite Belt in the Western Block of the North China Craton. *Lithos* **2011**, *122*, 25–38. [CrossRef]
53. Peng, P.; Guo, J.H.; Windley, B.F.; Liu, F.; Chu, Z.; Zhai, M.G. Petrogenesis of Late Paleoproterozoic Liangcheng charnockites and S-type granites in the central-northern margin of the North China Craton: Implications for ridge subduction. *Precambrian Res.* **2012**, *222–223*, 107–123. [CrossRef]
54. Li, S.Z.; Zhao, G.C.; Sun, M. Paleoproterozoic amalgamation of the North China Craton and the assembly of the Columbia supercontinent. *Chin. Sci. Bull.* **2016**, *61*, 919–925. [CrossRef]

55. Wang, L.J.; Guo, J.H.; Yin, C.Q.; Peng, P. Petrogenesis of ca 1.95Ga meta-leucogranites from the Jining Complex in the Khondalite Belt, North China Craton: Water-fluxed melting of metasedimentary rocks. *Precambrian Res.* **2017**, *303*, 355–371. [CrossRef]
56. Liu, K.X. *Tectonic Evolution of Alxa Block From the Proterozoic to Early Paleozoic*; Lanzhou University: Lanzhou, China, 2014.
57. Bu, W.R.; Wang, T.Y.; Ma, Y.J. Characteristics and tectonic environment of MesoProterozoic granitoid rocks in western section of northern margin of the North China Craton. *Acta Petrol. Sin.* **2001**, *17*, 609–616.
58. Duan, J.; Li, C.S.; Qian, Z.Z.; Jiao, J.G. Geochronological and geochemical constraints on the petrogenesis and tectonic significance of Paleozoic dolerite dykes in the southern margin of Alxa Block, North China Craton. *J. Asian Earth Sci.* **2015**, *111*, 244–253. [CrossRef]
59. Zhang, L.Q.; Zhang, H.F.; Zhang, S.S.; Xiong, Z.L.; Luo, B.J.; Yang, H.; Pan, F.B.; Zhou, X.C.; Xu, W.C.; Guo, L. Lithospheric delamination in post-collisional setting: Evidence from in trusive magmatism from the North Qilian orogen to southern margin of the Alxa block, NW China. *Lithos* **2017**, *288–299*, 20–34. [CrossRef]
60. Zhu, Z.Y.; Campbell, I.H.; Allen, C.M.; Burnhama, A.D. S-type granites: Their origin and distribution through time as determined from detrital zircons. *Earth Planet. Sci. Lett.* **2020**, *536*, 116140. [CrossRef]
61. Zhang, Y.Q. *The Geochemistry and Tectonic Significance of Granitoid-Dioritoid Rocks in Thewestern of Langshan Mt., Inner Mongolia*; Lanzhou University: Lanzhou, China, 2012.
62. Zhang, Y.Q.; Liu, J.J. Zircon U-Pb age of the quartz diorite in North Daqing mountains, central Inner Mongolia. *Geol. Miner. Resour. South China* **2004**, *00*, 22–27.
63. Li, Z.H.; Liu, X.M.; Dong, Y.P.; Xiao, Z.B. Geochemistry and zircon U-Pb age of the Paleoproterozoic syn-collisional granites in Helanshan region and its geological significance. *Acta Petrol. Sin.* **2013**, *29*, 2405–2415.
64. Yin, C.Q.; Zhao, G.C.; Sun, M.; Xia, X.P.; Wei, C.J.; Zhou, X.W.; Leung, W. LA-ICP-MS U-Pb zircon ages of the Qianlishan complex: Constrains on the evolution of the Khondalite Belt in the Western Block of the North China Craton. *Precambrian Res.* **2009**, *174*, 78–94. [CrossRef]
65. Zhu, X.H.; Chen, D.L.; Feng, Y.M.; Ren, Y.F.; Zhang, X. Granitic magmatism and tectonic evolution in the Qilian MountainRange in NW China: A review. *Earth Sci. Front.* **2022**, *29*, 241–260.
66. Wang, T.; Wang, X.X.; Tian, W.; Zhang, C.L.; Li, W.P.; Li, J. North Qinling Paleozoic granite associations and their variation in space and time: Implications for orogenic processes in the orogens of central China. *Sci. China Ser. D Earth Sci.* **2009**, *52*, 949–971. [CrossRef]
67. Shi, G.Z.; Wauschkuhn, B.; Ratschbacher, L.; Shen, C.B.; Fu, H.Y.; Frölich, S. Zircon-based proxies for source-rock prediction in provenance analysis: A case study using Upper Devonian sandstones, northern South China Block. *Sediment. Geol.* **2023**, *447*, 106366. [CrossRef]
68. Li, Z.H. Paleozoic Tectonic Evolution in the Helanshan Tectonic Belt: Constraints from U-Pb Geochronology of Detrital Zircon. Ph.D. Thesis, Northwest University, Xi'an, China, 2018.
69. Gong, J.H.; Zhang, J.X.; Yu, S.Y.; Li, H.K.; Hou, K.J. Ca. 2.5 Ga TTG rocks in the western Alxa Block and their implications. *Chin. Sci. Bull.* **2012**, *57*, 4064–4076. [CrossRef]
70. Liang, J.W.; Jie, C.; Zhao, K.Q.; Mei, H.P.; Liu, W.R.; Yang, L. Analysis of the provenance of the 8th member in Ordos Basin. *J. Xi'an Univ. Sci. Technol.* **2016**, *36*, 40–46.
71. Geng, Y.S.; Wang, X.S.; Shen, Q.H.; Wu, C.M. Redefinition of the Alax Group of Precambrian metamorphic basement in Alax region, Inner Mongolia. *Geol. China* **2006**, *33*, 138–145.
72. Geng, Y.S.; Wang, X.S.; Shen, Q.H.; Wu, C.M. Chronology of the Precambrian metamorphic series in the Alxa area, Inner Mongolia. *Geol. China* **2007**, *34*, 251–261.
73. Wang, Z.T.; Wang, G.H.; Zhang, W.J.; Wang, X.J. LA-ICP-MS zircon U-Pb dating and geochemical characteristics of the Silurian granodiorite in the southern margin of Alxa Block, China. *J. Chengdu Univ. Technol. Sci. Technol. Ed.* **2022**, *49*, 586–600.
74. Gan, D.B.; Zeng, R.Y.; Su, H.; Guan, Y.H. Geochronology, geochemistry and geological significance of the Early Carboniferous granite porphyry from the Beidashan area, Alxa block. *Chin. J. Geol.* **2023**, *58*, 556–579.
75. Wang, H.L.; He, S.P.; Chen, J.L.; Xu, X.Y.; Sun, Y.; Diwu, C.R. LA-ICPMS dating of zircon U-Pb and its tectonic significance of Maxianshan granitoid intrusive complex, Gansu province. *Acta Geol. Sin.* **2007**, *81*, 72.
76. Xu, X.Y.; Wang, H.L.; Chen, J.L.; He, S.P.; Wu, P.; Gao, T. Zircon U-Pb dating and petrogenesis of Xinglongshan Groupbasic volcanic rocks at eastern segment of Middle Qilian Mts. *Acta Petrol. Sin.* **2008**, *24*, 827–840.
77. He, D.F.; Bao, H.P.; Sun, F.Y.; Zhang, C.; Kai, B.; Xu, Y.; Cheng, X.; Zhai, Y. Geologic structure and genetic mechanism for the central uplift in the Ordos Basin. *Chin. J. Geol.* **2020**, *55*, 627–656.
78. Geng, Y.S.; Wang, X.S.; Shen, Q.H.; Wu, C.M. The discovery of Neoproterozoic Jinningian deformed granites in Alxa area and its significance. *Acta Petrol. Et Mineral.* **2002**, *21*, 412–420.
79. Geng, Y.S.; Wang, X.S.; Wu, C.M.; Zhou, X.W. Late-Paleoproterozoic tectonothermal events of the metamorphic basement in Alxa area: Evidence from geochronology. *Acta Petrol. Sin.* **2010**, *26*, 1159–1170.
80. Dan, W.; Li, X.H.; Wang, Q.; Wang, X.C.; Liu, Y. Neoproterozoic S-type granites in the Alxa Block, westernmost North China and tectonic implications: In situ zircon U-Pb-Hf-O isotopic and geochemical constraints. *Am. J. Sci.* **2014**, *314*, 110–153. [CrossRef]

81. Darby, B.J.; Gehrels, G. Detrital zircon referesnce for the North China block. *J. Asian Earth Sci.* **2006**, *26*, 637–648. [CrossRef]
82. Xia, Y.Q.; Fu, S.Y.; Huang, D.J.; Hu, J.L.; Chen, H.D.; Liu, X.P.; Wang, F.; Zhang, C.G.; Liu, L.; Chen, A.Q. Characteristics and control factors of carboniferous Yanghugou formation tight sandstone reservoir in western Ordos Basin. *Mineral. Petrol.* **2023**, *43*, 82–94.